

Physics-informed generative model for drug-like molecule conformers

David C. Williams* and Neil Inala*

Nobias Therapeutics

Abstract

We present a diffusion-based, generative model for conformer generation. Our model is focused on the reproduction of bonded structure and is constructed from the associated terms traditionally found in classical force fields to ensure a physically relevant representation. Techniques in deep learning are used to infer atom typing and geometric parameters from a training set. Conformer sampling is achieved by taking advantage of recent advancements in diffusion-based generation. By training on large, synthetic data sets of diverse, drug-like molecules optimized with the semiempirical GFN2-xTB method, high accuracy is achieved for bonded parameters, exceeding that of conventional, knowledge-based methods. Results are also compared to experimental structures from the Protein Databank (PDB) and Cambridge Structural Database (CSD).

Introduction

Conformer generation is the process of identifying a valid and useful set of atomic coordinates for a given molecule. Since so many tools in computational chemistry rely on atomic coordinates, it plays an important role in structure-based drug-discovery.¹ As such, several different methods for conformer generation have been developed and refined over the years,

each with their own advantages and disadvantages, but all with the general goal of providing a tool of sufficient quality for down-stream computation work such as protein docking.²⁻¹⁰

In a broad sense, we can define a valid conformer for a target molecule as a local minima in potential energy. As a practical matter, we could also insist that any such local energy minima be somewhat close in energy to a global minimum. There are still ambiguities, however, since the energy of a molecule is influenced by its environment, such as whether the molecule is solvated, in some type of solid form, or bound to a protein. In addition, from some perspectives, the (Gibbs) free energy is a more appropriate measure.

To help address these ambiguities, consider the bonded parameters of a molecule, such as bond lengths, bond angles, and torsions (Fig. 1). We generally expect such parameters to be weakly dependent on environment, a tendency reflected in the "1-4" exclusion for pair energies found in many classical force field parameterizations.¹¹⁻¹³ As such, an accurate reproduction of these bonded parameters could be considered a defining characteristic of a valid molecule conformer, independent of environment.

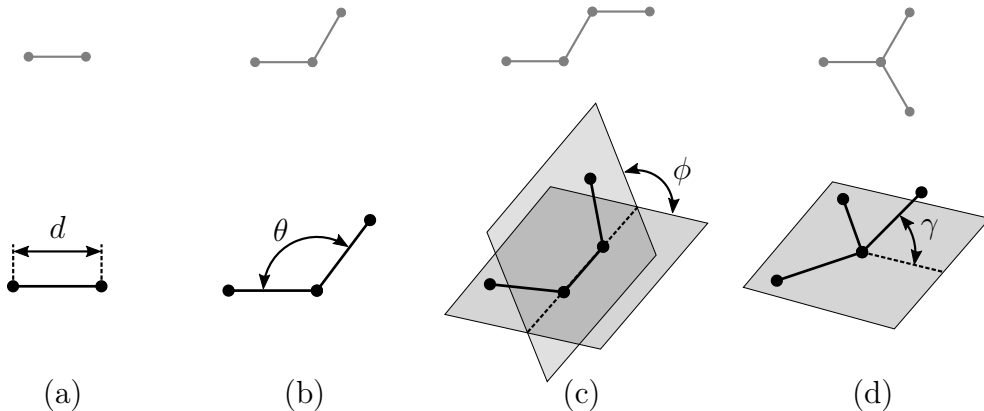


Figure 1: Force fields typically include bonded terms associated with (a) bond lengths, (b) bond angles, (c) proper torsions, and (d) improper torsions. Each term has an associated subgraph topology and a single characteristic property.

Note that proper torsions are typically parameterized as periodic, such that each as-

sociated term has an equally spaced set of favored values of torsion angle ϕ . Thus, it is possible for a molecule to exhibit multiple conformers with identical bonded parameters by sampling among a set of favored values of ϕ , a property we shall refer to as *torsional freedom*. Many docking algorithms take advantage of torsional freedom to sample ligand poses by manipulating proper torsion angles along with overall translation and rotation.^{4,14-17}

From this point of view, when developing a conformer generation algorithm, one could proceed with the assumption that a reproduction of bonded terms is the primary goal, with the sampling of torsional freedom as secondary, the latter being dependent on the molecular environment and target application. This approach is an advantage for models that rely on data sets for training, because the availability of experimental data on molecular conformers is limited. If we instead rely on synthetic data, we are limited to the assumptions used in constructing such data sets. For example, the public data sets used to train the model described in this work were generated under conditions of a vacuum, an environment that is unnatural for a drug-like molecule.

It should be emphasized, however, that sampling torsional freedom is a stated goal of most conformer solutions,^{5,6} since many applications, especially in drug development, are primarily concerned with a specific molecule environment (water solvent) and many do not perform their own independent, torsional sampling. For such applications, the model presented here will likely require additional downstream processing to be useful.

The atoms associated with bonded parameters are separated by no more than three bonds (Fig. 1). The distance between atoms separated by four or more bonds is therefore not constrained by a single bonded term. Such atom pairs will be referred to as *nonbonded*. In general, torsional freedom allows the distances between nonbonded atom pairs to vary.

Rings can pose several challenges. Because a cycle of atoms must be closed, constraints are imposed on bond angles. For non-aromatic systems, these constraints can often be satisfied in multiple ways, introducing different categories of corner folding (such as the “chair” and “twist boat” conformations of cyclohexane¹⁸). The situation becomes more complicated

for polycyclic systems. A successful conformer generator must be able to sample from the various possibilities, within some reasonable energy window.

Macrocycles impose constraints on torsional freedom that can be challenging to accommodate algorithmically.⁸

In addition to locating energy minima, a useful conformer generator needs to be able to distinguish between stable isomers. The two most important are chirality^{19,20} and cis/trans isomerism.²¹

Several algorithmic approaches to conformer generation have been developed over the years. CORINA,² one of the first commercial offerings, uses a simple ansatz for bond lengths and bend angles combined with geometric rules and backtracking, with a particular focus on the difficult problem of ring systems. FROG⁹ employs a template library for ring systems interconnected using canonical bond lengths and angles, followed by torsional freedom sampling via Monte Carlo. DG-AMMOS¹⁰ employs a hybrid Krylov solver for distance geometry²² followed by force-field minimization, and makes no attempt at sampling torsional freedom. In contrast, the OMEGA toolkit^{6,23} specializes in targeted sampling of torsional freedom, and employs a fragment library combined with rules-based sampling for bonded parameters. Balloon³ is a conformer generator based on a multiobjective genetic algorithm. ETKDGv3^{5,8} is a knowledge-based generator provided by RDKit²⁴ based on distance geometry, with additional heuristics targeted at macrocycles. ETKDGv3 is commonly followed by force-field optimization to improve the accuracy of bonded parameters,⁵ an option conveniently provided by RDKit.

The problem of conformer generation has been an attractive target for the machine-learning community, due to the broad availability of cheminformatics libraries, the approachable, geometric nature of the problem, and relevance in drug discovery. Many attempts, however, have focused on technological advancement at the detriment of physical viability and utility, perhaps due to lack of appropriate domain knowledge. Several strategies have been employed, such as energy gradients,²⁵⁻²⁷ Gibbs sampling,²⁸ and conditional variational

encoders.^{29,30} The drawback of these approaches is that the energy of disordered molecule systems is difficult to characterize directly due to singularities and large energy barriers. GeoMol³¹ learns local structure and applies incremental construction. Since incremental construction is poorly suited to cycles, it fails to reproduce all but the simplest ring systems.

GeoDiff³² is a stochastic diffusion model. It follows conventions most closely related to "denoising diffusion probabilistic models"³³ (an approach developed for images), employs around 800,000 independent parameters, and relies on an uncharacteristically large number of steps for generation. GeoDiff attempts to learn explicit values for the distances between nonbonded atom pairs, a physically ambiguous quantity due to torsional freedom. This requirement likely contributes to a high level of computational complexity.

Torsional diffusion³⁴ is a generative model designed to explore torsional freedom. It relies entirely on the ETKDGv3⁸ algorithm for the difficult task of establishing the bonded parameters. To make the task more tractable, macrocycles are ignored, and molecules are limited to no more than seven free torsion angles. The authors trained this model to reproduce the torsional freedom of a synthetic data set of drug-like molecule conformers selected arbitrarily and generated in a vacuum,³⁵ an objective of questionable physical relevance.

Diffusion-based generation

Diffusion is a machine-learning technique introduced in 2015³⁶ and more recently the subject of groundbreaking research in image generation.^{33,37} The results have been impressive enough to spawn several commercial endeavors^{38,39} and capture the imagination of the general public.⁴⁰

The methodology of diffusion-based generative modeling is described in detail elsewhere^{41,42} and only the general principles are summarized here. By applying noise of varying amounts to a suitable data set, it is possible to train a "denoising" model that can take a system with noise and predict the original state. If properly prepared, a model of this type can be applied in a series of sequential steps to extract a random sample from pure noise. If the

data used for training are labeled in some fashion, and if those labels are incorporated in the model during training, a diffusion model can be instructed to bias generation to match a given set of labels, producing a result corresponding to instructions.

Because of its success, diffusion-based models have been the subject of considerable study⁴³⁻⁴⁵ and many applications outside of image generation have been developed.⁴⁶⁻⁵⁰ Various approaches to diffusion have been proposed, from DDPM (denoising diffusion probabilistic models),³³ VDM (variational diffusion models),⁴⁴ score-based modeling,⁴⁵ and LDM (latent diffusion models),⁵¹ to name a few. The approach used in this work is based on recent developments on formulating a universal framework for describing diffusion-based models⁴¹ around the concept of denoising score matching.⁵²

Extending diffusion-based techniques developed for images to molecule conformer generation appears simple on the surface, however there are important differences. In images, each element \mathbf{x}_i of the model space corresponds to the color of a pixel, and the size of $\{\mathbf{x}_i\}$ depends on the number of pixels in the image to be generated. For a molecule, the size of $\{\mathbf{x}_i\}$ corresponds to the number of atoms, and each element corresponds to the projection of a given atom position onto an arbitrary Cartesian reference system. Whereas the solution $\{\mathbf{x}_i\}$ for an image is bounded to the color space of the problem (with a universal origin and scale), the solution $\{\mathbf{x}_i\}$ of a molecule need only be internally consistent and should otherwise be translationally and rotationally invariant.

Described in this article is a novel method of conformer generation using a physics-informed, denoising model (PIDM). By taking advantage of established methods employed in classical force fields, the intent is to construct a model that is accessible, transferable and robust. Suitable training sets and benchmark criteria are chosen with these same concepts in mind. Building upon recent theoretical advancements,⁴¹ both deterministic and stochastic methods of generation are explored. A form of guided generation is demonstrated as a means of exploring torsional freedom.

Limitations

Neglecting to appropriately sample torsional freedom will produce conformers that are inadequate for applications that do not perform their own sampling, such as rigid ligand docking or 3D pharmacophore modeling, unless additional processing of some kind is applied.

Conformer generation for molecules with chemical groups or atom types outside the training set may perform poorly or fail. Molecules with certain challenging topologies, such as a central ring with several large branches, may perform poorly (see Fig. 12). Conformer quality is expected to degrade as molecules grow in size beyond ~ 200 heavy atoms.

Methods

Our goal is to provide a method that can be used to generate realistic conformers, independent of torsional freedom, for any drug-like molecule when provided with just the atom composition, connectivity, and isomer (chirality, cis/trans) identity. Emphasis is placed on the reproduction of bonded terms and the preservation of given chirality and cis/trans isomerism.

Denoising Function

As discussed earlier, diffusion-based models can be generalized around the concept of denoising. To that end, we may represent our model as a denoising function D that yields an estimate of the actual coordinates \mathbf{x} of the atoms of a molecule when provided with coordinates that have been perturbed by a centered, uncorrelated Gaussian of width σ

$$\mathbf{x} \approx D(\mathcal{N}(\mathbf{x}; 0, \sigma^2 \mathbf{I}), \sigma; \zeta), \quad (1)$$

where ζ represents the composition of the molecule (*i.e.* its atom types, connectivity, and isomer identity). The behavior of D is controlled by a set of internal parameters that are

in a new embedding space that captures information on connectivity. No information on atom coordinates is used at this stage.

The GATv2 graph attention network contained in each layer is constructed by associating each molecular bond with a graph edge. Self edges are not included since they would not reflect an appropriate physical analog (a self edge would be equivalent to a bond to an identical atom). Instead, the input to the graph network is concatenated to the output in order to preserve a form of atom self-identity. This concatenation is fed into a feed-forward network to form the output of each layer.

It should be noted that the edges used in the graph layers include no labeling, such as bond order. Such labeling was not deemed necessary since connectivity alone in combination with atomic number, formal charge, and hybridization should provide sufficient context to describe relevant chemistry.⁵⁴

Each of the bonded components have their own challenges and are individually described in what follows.

The purpose of the “bond” component is to calculate a correction to atom positions to account for the expected distance $|\boldsymbol{\delta}|$ between bonded atoms:

$$\boldsymbol{\delta}_{ij} \doteq \mathbf{x}_j - \mathbf{x}_i. \quad (2)$$

In this notation, we are using the subscript to refer to the Cartesian coordinates of the corresponding atom. The correction $\boldsymbol{\Delta}^d$, a vector in Cartesian space, is calculated as a displacement along $\boldsymbol{\delta}$ separately for each of the two atoms associated with the bond. The magnitudes of the displacements are implemented, using a multilayer perceptron (MLP), as an arbitrary function of the current distance, the characteristic Gaussian width of the noise, and the associated atom embeddings \mathbf{a} . The correction applied to each atom of a bond can thus be described, under a certain convention, as the following:

$$[-\boldsymbol{\Delta}_i^d, \boldsymbol{\Delta}_j^d] = \frac{1}{2} \text{MLP}(|\boldsymbol{\delta}_{ij}|, \sigma; \mathbf{a}_i, \mathbf{a}_j) \hat{\boldsymbol{\delta}}_{ij}, \quad (3)$$

where $\hat{\boldsymbol{\delta}}_{ij}$ is the normal vector along the direction of $\boldsymbol{\delta}_{ij}$. In the implementation, the input to the MLP is a concatenation of the function variables and parameters, after suitable weighting. A similar method is used for the other components described below.

For the ‘‘bend’’ component, a complication is that the target bend angle depends on whether the corresponding three atoms are a part of a ring, and if so, the size of the ring. One of the unfortunate weaknesses of message-passing, graph convolution networks, of which GATv2 is a member, is the inability to detect cycles.⁵⁵

To work around this weakness, a bit-encoded integer is used to enumerate the size and number of rings which belong to all three of the atoms of the bend, for ring sizes up to and including 6 (it is possible for a bend to be embedded in more than one ring). This integer is mapped to an embedding \mathbf{c}_{ijk} . The bend angle correction $\boldsymbol{\Delta}^\theta$ applied to the two outer atoms then follows a scheme similar to the bond correction:

$$[-\boldsymbol{\Delta}_i^\theta, \boldsymbol{\Delta}_k^\theta] = \frac{1}{2} \text{MLP} (|\boldsymbol{\delta}_{ik}|, \sigma; \mathbf{a}_i, \mathbf{a}_j, \mathbf{a}_k, \mathbf{c}_{ijk}) \hat{\boldsymbol{\delta}}_{ik}. \quad (4)$$

Notice that Eq. 4 uses the distance between the outer two atoms instead of the bend opening angle (Fig. 3). This is a deliberate choice. Unlike the opening angle, the distance is unbounded, and thus more numerically tractable. Eliminating the dependence on the position of the central atom also removes some noise, especially when σ approaches the associated bond lengths. For similar reasons, the correction for atom position is calculated along the vector between the two outer atoms, rather than as a rotation around the central atom.

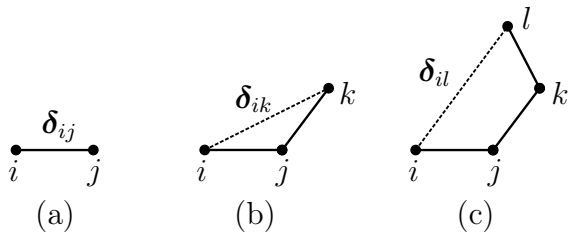


Figure 3: Characterizing bonded terms using atom distances $|\delta|$. Shown are (a) bonds, (b) bends, and (c) proper torsions.

A similar strategy is used for the “proper torsion” component

$$\left[-\Delta_i^\phi, \Delta_l^\phi\right] = \frac{1}{2} \text{MLP}(|\delta_{il}|, \phi_{ijkl}, \sigma; \mathbf{a}_i, \mathbf{a}_j, \mathbf{a}_k, \mathbf{a}_l) \hat{\delta}_{il}, \quad (5)$$

where the proper torsion angle ϕ is included as an argument to the MLP. The angle is useful because proper torsions, as discussed earlier, typically have multiple, favored values of ϕ , each of which will be characterized by a corresponding distance $|\delta_{il}|$ (see Fig. 1c). To avoid discontinuities in the modulo of ϕ , the concatenation for the input of the MLP uses $[\cos \phi, \sin \phi]$ in place of ϕ .

Improper torsions, used by force-field parameterizations primarily as a means to enforce planarity in conjugated systems, are already constrained by bond lengths and bend angles. There is, however, an important connection with chirality and the sign of the improper torsion angle γ (Fig. 4).

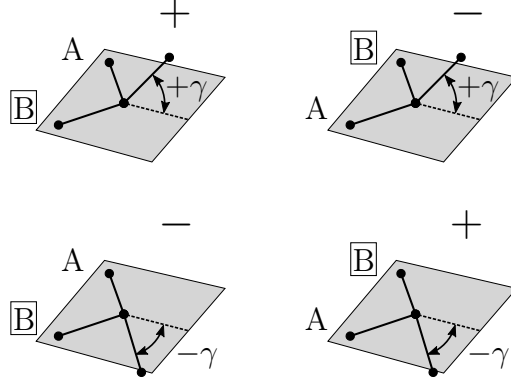


Figure 4: The sign of chirality in terms of an improper torsion angle. The sign depends on whether a neighboring atom is above or below the plane formed by the other three atoms. The sign changes if any two neighboring atoms are swapped.

Consider an improper torsion centered on atom i , with a plane defined in combination with atoms j and k , and a fourth atom l for which we calculate γ . We can define a distance d_{\parallel} along the plane and a signed distance d_{\perp} out of the plane:

$$\begin{aligned} d_{\parallel,ijkl} &= \boldsymbol{\delta}_{il} \cdot \hat{\boldsymbol{\delta}}_{\parallel,ijk} \\ d_{\perp,ijkl} &= \boldsymbol{\delta}_{il} \cdot \hat{\boldsymbol{\delta}}_{\perp,ijk}, \end{aligned} \quad (6)$$

where

$$\begin{aligned} \boldsymbol{\delta}_{\parallel,ijk} &\doteq -(\boldsymbol{\delta}_{ij} + \boldsymbol{\delta}_{ik}) \\ \boldsymbol{\delta}_{\perp,ijk} &\doteq \chi_{ijkl} (\boldsymbol{\delta}_{ij} \times \boldsymbol{\delta}_{ik}), \end{aligned} \quad (7)$$

and where $\chi_{ijkl} = \pm 1$ is the target chirality. The ‘‘chirality’’ bonded component of the model uses the above to enforce a given signed distance out of the plane, by displacing atoms i and l :

$$[-\boldsymbol{\Delta}_i^t, \boldsymbol{\Delta}_l^t] = \frac{1}{2} \text{MLP} (d_{\perp,ijkl}, d_{\parallel,ijkl}, \sigma; \mathbf{a}_i, \mathbf{a}_j, \mathbf{a}_k, \mathbf{a}_l) \hat{\boldsymbol{\delta}}_{\perp,ijk}. \quad (8)$$

The above term is used for all three combinations of the atoms in an improper torsion, such that the total correction for the central atom is a vector sum of the three. For a chiral atom

with four bonded atoms, there are four improper torsions, and thus twelve terms in total.

The ‘‘cis/trans’’ component is the last of five and is designed to enforce explicit cis/trans isomerism associated with double bonds. The planer structures typically associated with double bonds allow two possible configurations for the associated proper torsions, corresponding to $\phi \simeq 0$ and $\phi \simeq \pm\pi$. Rather than use the angle ϕ directly, we introduce, for a more robust solution, the average vector between the inner and outer atoms of a proper torsion:

$$\boldsymbol{\delta}_{ijkl} \doteq \frac{1}{2} (\mathbf{x}_j + \mathbf{x}_l - \mathbf{x}_i - \mathbf{x}_k), \quad (9)$$

which is equivalent to the vector between the center of the segment connecting the outer atoms and the center of the bond connecting the inner atoms. The implementation of the component can be expressed as:

$$[-\boldsymbol{\Delta}_i^c, \boldsymbol{\Delta}_j^c] = [-\boldsymbol{\Delta}_l^c, \boldsymbol{\Delta}_k^c] = \frac{1}{2} \text{MLP} (|\boldsymbol{\delta}_{ijkl}|, \chi_{ijkl}, \sigma; \mathbf{a}_i, \mathbf{a}_j, \mathbf{a}_k, \mathbf{a}_l) \hat{\boldsymbol{\delta}}_{ijkl}, \quad (10)$$

where χ_{ijkl} is equal to -1 ($+1$) for the target cis (trans) state and the same correction is applied to pairs of atoms. Depending on the chemistry, each cis/trans group can be associated with up to four proper torsions, in which case each outer atom receives a vector sum of two corrections and the two inner atoms each receive four.

The final output of the model is an estimate of the unsmeared coordinates and can be expressed symbolically as the sum of all contributions:

$$D(\mathbf{x}, \sigma) = \mathbf{x} + \sum_{\text{bonds}} \boldsymbol{\Delta}^d + \sum_{\text{bend}} \boldsymbol{\Delta}^\theta + \sum_{\text{proper}} \boldsymbol{\Delta}^\phi + \sum_{\text{chirality}} \boldsymbol{\Delta}^t + \sum_{\text{cis/trans}} \boldsymbol{\Delta}^c. \quad (11)$$

Here the various arguments and indices have been suppressed for clarity. By training on the vector sum of the five components, the model can learn to adapt to correlated behavior.

As consistent with our goals, the denoising function of Eq. 11 makes no attempt to predict the distance between nonbonded pairs of atoms.

For the models reported here, an atom embedding of dimension 50 is used throughout. Four graph transformer layers were employed. The result is a model with a total of 135,080 parameters (weights), with 63,480 reserved for the molecule graph and 71,240 in the geometry components.

Training

For the purposes of training, we choose to evenly sample from a canonical set $\{\sigma_1 \dots \sigma_N\}$:

$$\sigma_i = \begin{cases} \left(\sigma_{\max}^{1/\rho} + \frac{i-1}{N-1} \left(\sigma_{\min}^{1/\rho} - \sigma_{\max}^{1/\rho} \right) \right)^\rho & 1 \leq i < N \\ 0 & i = N \end{cases}. \quad (12)$$

The total loss is calculated as the weighted sum of the contribution from each sample σ_i

$$\mathcal{L} = \sum_{i=1}^N \frac{1}{\sqrt{\sigma_i^2 + \epsilon^2}} \mathcal{L}(\sigma_i) \quad (13)$$

with

$$\mathcal{L}(\sigma) = \mathbb{E}_{\mathbf{x} \sim \text{data}, \mathbf{n} \sim \mathcal{N}(0, \sigma^2 \mathbf{I})} \|\mathbf{D}(\mathbf{x} + \mathbf{n}, \sigma) - \mathbf{x}\|_2^2, \quad (14)$$

and where \mathbb{E} is the expected value obtained from the training data after applying random Gaussian sampling. Standard techniques such as the AdamW algorithm⁵⁶ and mini batches were used to establish model weights that minimize \mathcal{L} . Hyperparameter values of $N = 100$, $\sigma_{\max} = 8\text{\AA}$, $\sigma_{\min} = 10^{-5}\text{\AA}$, $\epsilon = 10^{-5}\text{\AA}$, and $\rho = 6$ were found to produce satisfactory results.

Concerning data sources for training, a large, representative sample of drug-like molecules would be ideal. For a meaningful benchmark, a well-quantified baseline is also desirable. Two publically available, synthetic data sets come to mind: QMugs⁵⁷ and GEOM-drugs.³⁵ Both contain samples of several hundred thousand drug-like molecules with conformers optimized (in vacuum) using the GFN2-xTB semiempirical quantum mechanical method.^{58,59} Statistics on both sets are shown in Table 1. Molecular weight and estimated LogP distributions are

shown in Fig. 5.

To measure the similarity of two compounds, we employ the ECFP6 (extended-connectivity) fingerprint, as implemented by RDKit²⁴ and folded to 1024 bits. Using a relatively permissive Tanimoto threshold of 0.9, we find that only 5.6% of the compounds in QMugs overlap with those in GEOM-drugs. This increases to 6.3% if the threshold is lowered to 0.8.

Table 1: Statistics on the QMugs⁵⁷ and GEOM-drugs³⁵ data sets, after quality filtering.

Quantity	QMugs	GEOM-drugs
Molecules	665,911	301,821
Molecule atoms	36,679,641	13,378,196
Molecule bonds	38,640,204	13,981,212
Molecule angles	67,526,717	24,090,418
Proper torsions	98,098,868	33,819,616
Improper torsions	32,187,240	11,220,749
Proper torsions with cis/trans isomerism	237,879	149,831
Improper torsions with chirality	2,864,349	540,979
Conformers	1,992,984	30,906,135
Conformer atoms (nodes)	110,044,367	1,599,467,582
Conformer bonds (edges)	202,017,554	1,658,998,071
Average molecular weight	433.3	355.5
Average number of heavy atoms	30.6	24.8

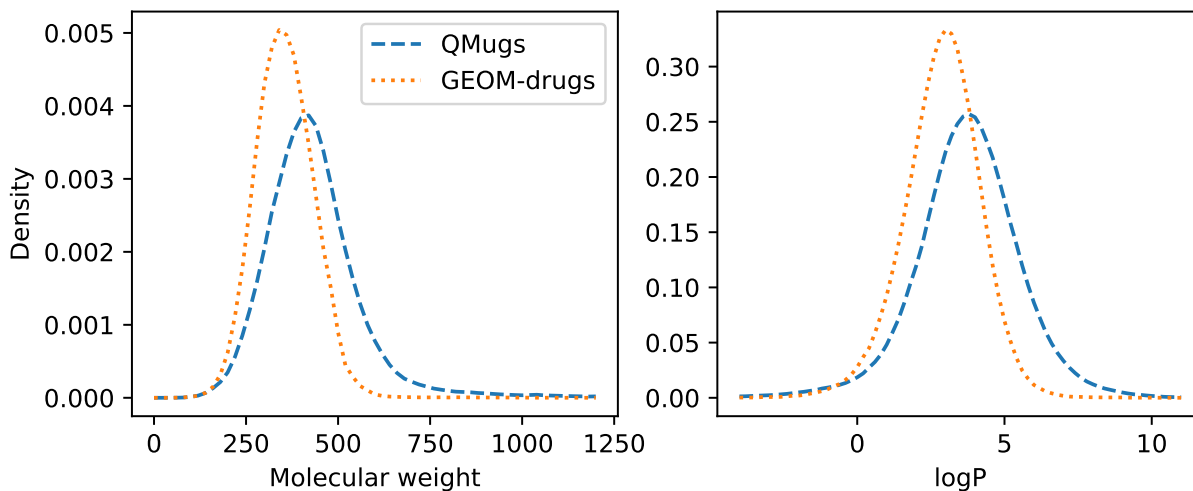


Figure 5: The distribution of molecular weight (left) and logP (right) for two datasets. The logP value is estimated using the Crippen algorithm.⁶⁰

The processing used by their authors to create the two data sets are somewhat different.

For the QMugs data set,⁵⁷ molecules extracted from the ChEMBL database⁶¹ were charge neutralized, and a limit of three conformers are selected for each molecule. Radical species were also removed. The result is a total of 28 distinct atom types, as enumerated by element, formal charge, and hybridization. The total number of edges, when counting by conformer, is approximately 200 million.

For the GEOM-drugs data set,³⁵ molecules were taken from the AI Cures conference open challenge^{62,63} and MoleculeNet.⁶⁴ No molecule charge neutralization was attempted, which is somewhat unnatural, given that the conformers were generated and optimized in vacuum. The result is a total of 64 distinct atom types, a superset of those found in the QMugs data set. Conformer generation was more liberal, resulting in an average of around 100 conformers per molecule, or a total of nearly 1.7 billion edges.

Performing quantum-level optimization of charged species in vacuum can increase the likelihood of artifacts, as bonds are broken and created. For the purposes of this study, the conformers provided by GEOM-drugs for each molecule was checked for strict consistency at the graph level, and if any discrepancy was detected, the molecule was removed from consideration. This affected about 2% of the data set.

It should be noted that the conformers in the QMugs data set are stored in standard SDF format. This limits coordinate resolution to 10^{-4}\AA . The GEOM-drugs data set does not suffer from this limitation.

Both data sets are randomly divided into training (80%), validation (10%), and test (10%) subsets. One version of the model is trained on the QMugs training subset using a fixed schedule of 100 epochs, corresponding to approximately 1.6 million steps, with no evidence of overtraining (Fig. 6a). The loss as calculated independently for the validation set during training is remarkably consistent with the training loss.

A second version of the model is trained on the GEOM-drugs training subset using a fixed schedule of 25 epochs, corresponding to approximately 6.2 million steps. There is also little evidence of overtraining and no apparent difference between training and validation

losses (Fig. 6b).

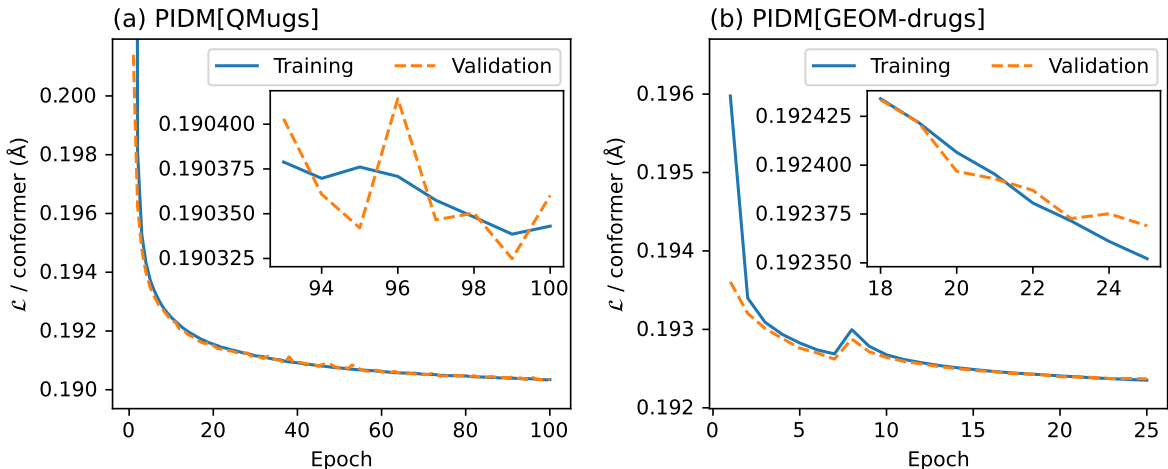


Figure 6: Loss per conformer as calculated during model training for (a) QMugs and (b) GEOM-drugs. Plotted are losses calculated for the training subset and for an independent validation set of 1/8 the size.

Probing the models

Perhaps the most direct way to judge the quality of a trained model is to apply it in generation and inspect the resulting conformers. That task will be the subject of the following sections. Before doing so, it is instructive to probe the model structure using example compounds and infer characteristics of its learned behavior. Some examples are described below. Further examples are available in the Supporting Information.

Shown in Fig. 7 is the output of the bond component for an example alkane bond as a function of $|\delta_{ij}|$, calculated for various values of σ (see Eq. 3). As $|\delta_{ij}|$ increases, the model predicts larger corrections. This has the overall tendency of pulling bonded atoms closer together. As σ approaches zero, the correction vanishes once the correct bond length is achieved.

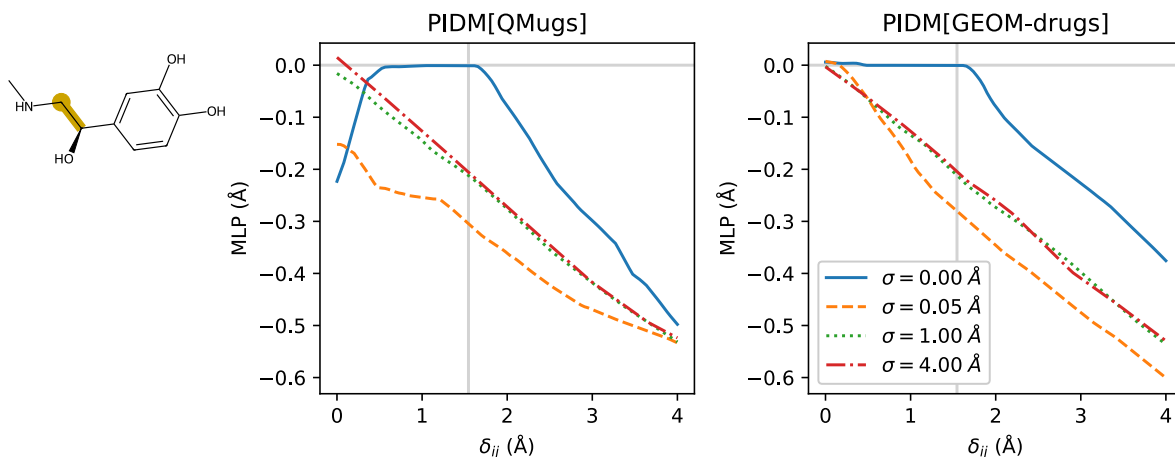


Figure 7: Example bond correction for the two models for an atom involved in an alkane bond in adrenaline. Corrections for various values of σ are plotted. The vertical gray line is the expected bond distance from a GFN2-xTB optimization.

Notice that the correction for the bond is smaller than required for that bond alone (that is, the correction falls well inside a line of unit slope). This is characteristic of the individual corrections learned by the model because the final result is the sum of all corrections. As a consequence, bonded components tend to act in concert.

An example of the output of the bend component is shown in Fig. 8. The example has a similar behavior to the bond, except there is more of a tendency to push atoms apart if they are too close. Presumably this is part of a compensating mechanism for the tendency of the bond component to pull atoms together.

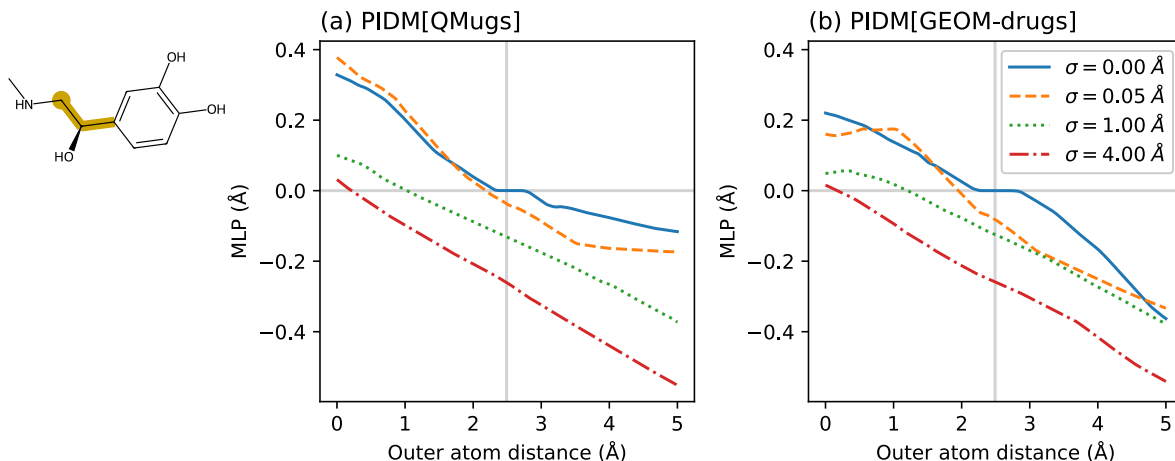


Figure 8: Example bend correction for the two models for an atom involved in the ethanol group of adrenaline. Corrections for various values of σ are plotted. The vertical gray line is the expected atom distance from a GFN2-xTB optimization.

Probes of the proper torsion, chirality, and cis/trans components are also revealing. Details can be found in the Supplemental Information.

Generation

We adopt a score-based, probability flow framework⁴⁵ in order to generate conformers from our trained model. As is typical in this approach, we consider a multidimensional Wiener process applied to molecule coordinates \mathbf{x} over a time interval $t \in [0, 1]$:

$$p_t(\mathbf{y}(t)|\mathbf{x}; \sigma(t)) = \mathcal{N}(\mathbf{y}(t); \mathbf{x}, \sigma(t)^2 \mathbf{I}), \quad (15)$$

where $\mathbf{y}(t)$ are the resulting random coordinates and where $\sigma(t)$ is a width schedule we are free to choose to suit our task with the only requirement that $\lim_{t \rightarrow 0} \sigma(t) = 0$. For generation, we start by sampling from a random Gaussian distribution $\mathcal{N}(0, \sigma(1)^2 \mathbf{I})$ as an approximation for $\mathbf{y}(1)$ and solve for the corresponding reverse process (denoising) to obtain $\mathbf{y}(0)$ as a candidate solution for \mathbf{x} .

To construct a solution for the reverse process, we identify the marginal distribution

$p(\mathbf{y}; \sigma)$ as

$$p(\mathbf{y}; \sigma) = \int p_t(\mathbf{y}|\mathbf{x}; \sigma) p(\mathbf{x}) d\mathbf{x}, \tag{16}$$

where the t dependence is implicit and $p(\mathbf{x})$ represents the marginal distribution of the training data. We can use $p(\mathbf{y}; \sigma)$ to express the time dependence of \mathbf{y} as a *probability flow* ODE:⁴¹

$$d\mathbf{y} = -\frac{d\sigma}{dt} \sigma \nabla_{\mathbf{y}} \log p(\mathbf{y}; \sigma) dt, \tag{17}$$

where $\nabla_{\mathbf{y}} \log p(\mathbf{y})$ is the *score function*. In a score-based framework, there is a direct relationship between the score function and our denoising model D :^{41,52}

$$\nabla_{\mathbf{y}} \log p_t(\mathbf{y}; \sigma) \approx \frac{1}{\sigma^2} (D(\mathbf{y}, \sigma; \boldsymbol{\zeta}) - \mathbf{y}), \tag{18}$$

where $\boldsymbol{\zeta}$ represents the molecular structure of interest. This important relation connects our denoising model to the conformer generation process.

In our implementation, we have selected a linear function $\sigma(t) = \alpha t$, where α is a scale parameter in units of Å. Applying this selection to Eq. 17 and 18 results in a simple form for the probability flow ODE:

$$\frac{d\mathbf{y}}{dt} = (\mathbf{y} - D(\mathbf{y}; \alpha t; \boldsymbol{\zeta})) / t. \tag{19}$$

Our conformer generation process is the numerical solution to this equation, calculated in steps of t in reverse, and using as initial conditions $\mathbf{y}(1) \sim \mathcal{N}(0, \alpha^2 \mathbf{I})$.

Inspired by work elsewhere,⁴¹ we solve Eq. 19 using Heun’s 2nd-order method, augmented by a form of backtracking (Algorithm 1). The backtracking provides an option to add additional noise to the generation process. We can begin by dividing the interval $[0, 1]$ into a fixed set of sequentially diminishing steps $\{t_i\}$ over which we iterate, to calculate a set of intermediate solutions $\{\mathbf{y}_i\}$. Instead of relying on solving along the connected, nonoverlapping intervals $t_{i+1} \leq t < t_i$, we can substitute modified values for the upper

bound t_i of each interval:

$$\begin{aligned}\tilde{t}_i &= \beta t_i \\ \tilde{\mathbf{y}}_i &\sim \mathcal{N}(\mathbf{y}_i; 0, \lambda^2 \alpha^2 t_i^2 (\beta^2 - 1))\end{aligned}\tag{20}$$

where $\beta \geq 1$ and $\lambda \geq 0$ are free parameters. This has the effect of introducing Gaussian noise at each step of the solution. For $\lambda = 1$, the amount of added noise compensates for the change in interval size.

Algorithm 1 Conformer generation.

```

1: procedure GENERATE( $D(\mathbf{y}, \sigma), \{t_i\}, \alpha, \beta, \lambda$ )
2:    $\mathbf{y} \leftarrow \mathcal{N}(0, \alpha^2 \mathbf{I})$  ▷ Prepare random initial state
3:   for  $i \leftarrow 1$  to  $|t|$  do
4:      $\tilde{t} \leftarrow \beta t_i$  ▷ Widen effective interval
5:      $\tilde{\mathbf{y}} \leftarrow \mathcal{N}(\mathbf{y}; 0, \lambda^2 \alpha^2 t_i^2 (\beta^2 - 1) \mathbf{I})$  ▷ Add noise
6:      $\mathbf{d}_1 \leftarrow (\tilde{\mathbf{y}} - D(\tilde{\mathbf{y}}, \alpha \tilde{t})) / \tilde{t}$  ▷ Evaluate  $d\mathbf{y}/dt$ 
7:      $\mathbf{y} \leftarrow \tilde{\mathbf{y}} + (t_{i+1} - \tilde{t}) \mathbf{d}_1$  ▷ Solve
8:     if  $t_{i+1} > 0$  then
9:        $\mathbf{d}_2 \leftarrow (\mathbf{y} - D(\mathbf{y}, \alpha t_{i+1})) / t_{i+1}$  ▷ Apply 2nd-order correction
10:       $\mathbf{y} \leftarrow \tilde{\mathbf{y}} + \frac{1}{2} (t_{i+1} - \tilde{t}) (\mathbf{d}_1 + \mathbf{d}_2)$ 
11:       $\mathbf{y} \leftarrow \mathbf{y} - \langle \mathbf{y} \rangle$  ▷ Remove center of mass
12:   return  $\mathbf{y}$ 

```

For reasons of convenience, we remove an overall center-of-mass during each generation step. This prevents solutions from slowing walking in coordinate space and helps with inspecting results. The correction is small and quality of output is not affected.

If we generate using $\lambda = 0$, no noise is added during the intermediate steps. In the language of diffusion-based models, we call this a “deterministic” approach, even though we still begin with a random initial state $\mathbf{y}(1)$. Combined with $\beta > 0$, the algorithm is equivalent to pretending that each intermediate value \mathbf{y}_i belongs to a solution sampled from a larger value of σ . This has the effect of overcorrecting, which improves accuracy in our case.

If we generate using $\lambda > 0$ and $\beta > 0$, we inject noise during each step of generation. This is referred to as a “stochastic” approach. Both stochastic and deterministic approaches have been used for image generation, with impressive results.^{33,41,43–45,65–67}

To apply our algorithm, we use an exponentially decreasing set $\{t_1 \dots t_N\}$ of a given size N and final step size t_ϵ :

$$t_i = \begin{cases} t_\epsilon^{i/(N-1)} & 1 \leq i < N \\ 0 & i = N \end{cases}. \quad (21)$$

The quality of generated output is reasonably stable for a large range of parameter values. The results reported here use $t_\epsilon = 0.0006$, $\alpha = 2.5 \text{ \AA}$, and $\beta = 5$. Quality improves marginally if the solution is calculated using more steps at a proportional cost in processing time. To quantify this trade off, we report on results for $N = 100, 200, \text{ and } 500$. We also report results for both deterministic ($\lambda = 0$) and stochastic ($\lambda = 1$) generation.

Results

Shown in Fig. 9 are random examples of generated conformers, using deterministic generation, 500 steps, and the model trained on QMugs (PIDM[QMugs]). Similar figures, generated under different conditions, such as stochastic generation or using PIDM[GEOM-drugs], are available in the Supporting Information, along with corresponding molecular structures files. Visual inspection alone does not reveal any apparent difference in conformer quality.

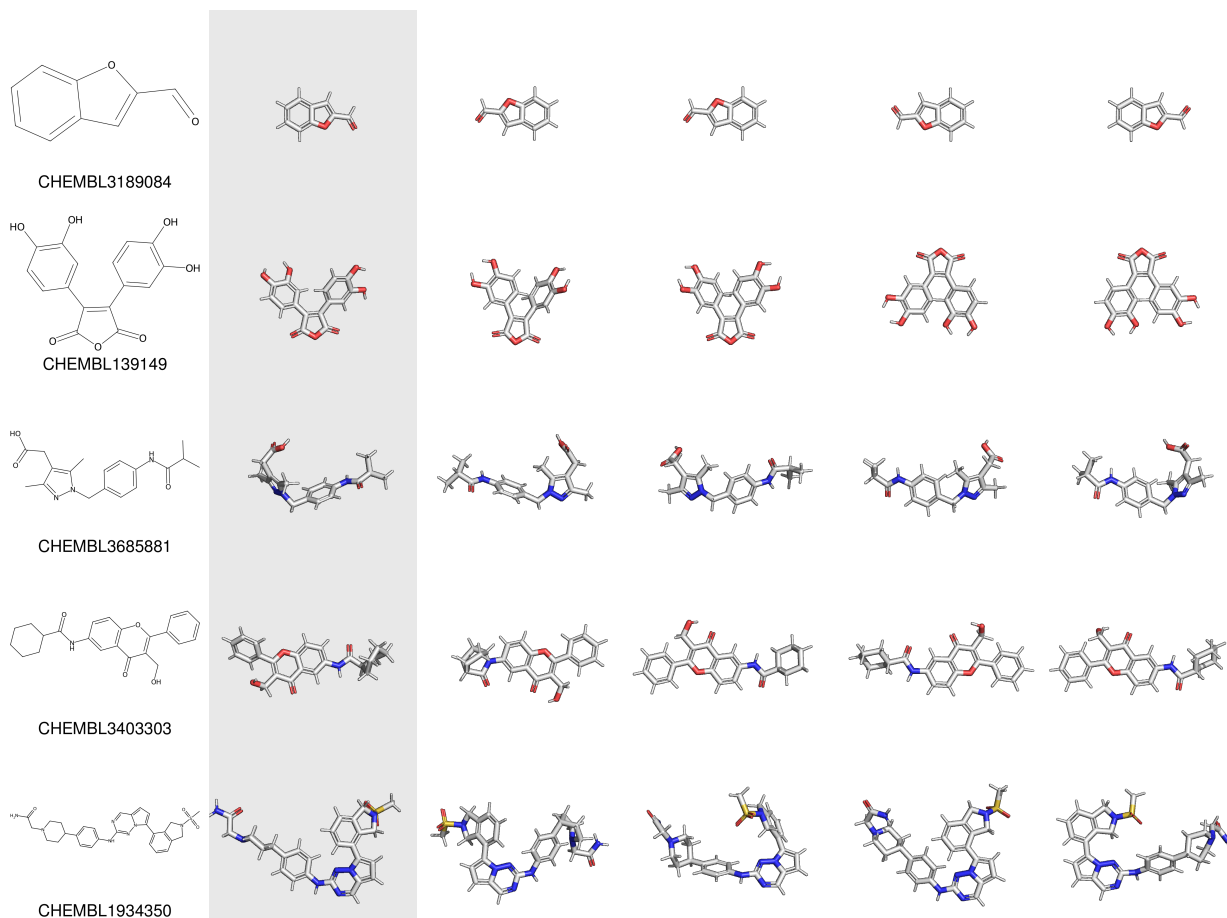


Figure 9: Example conformer output, for the model trained on QMugs, using deterministic generation and 500 steps, and for molecules randomly selected from an independent benchmark molecule set (see text for details). Shown in the second column from left (grey background) is the first conformer from QMugs. Shown on the right are four conformer outputs, selected randomly. All molecule renderings are oriented by principal component.

Shown in Fig. 10 are some selected examples of conformer generation. For each of these molecules, good quality conformers are generated the majority of the time. Sterols such as cholesterol contain fused ring systems whose conformation could not have been reliably generated without faithfully reproducing multiple chiralities. Large aromatic systems, such as naphthalene, generate as reasonably flat, even though our model does not contain the associated improper torsion terms. Complex, fused ring systems are also reliably reproduced, even those with bridges, such as artemether.

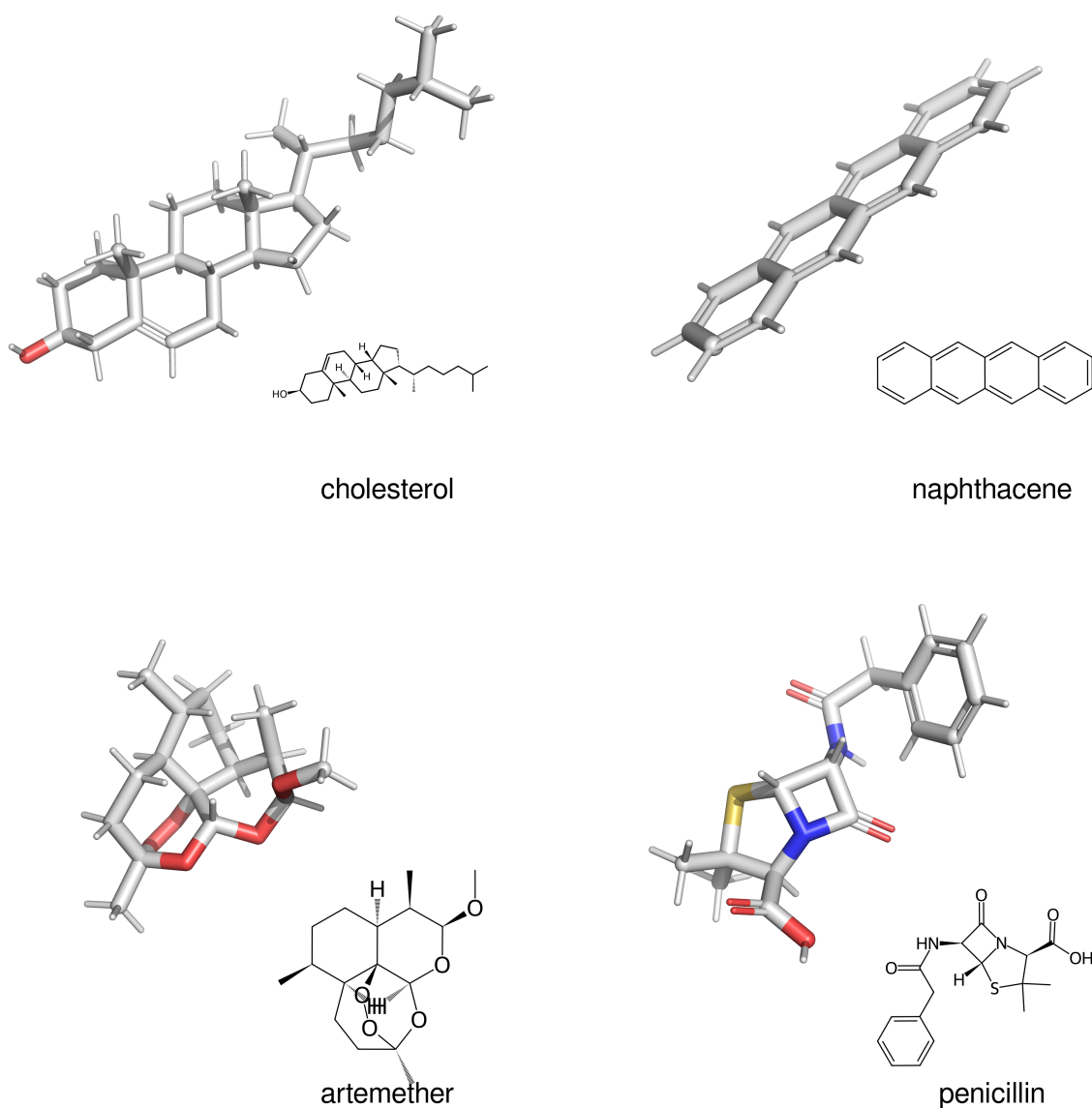


Figure 10: Select examples of conformer generation. These examples were generated using PIDM[QMugs] with 500 steps in the deterministic scheme.

One of the characteristics of deterministic generation is that the frames transition smoothly toward the final solution. This behavior is most apparent when generation is presented as an animation, samples of which are included in the Supporting Information. A static depiction of stages in the generation process is shown in Fig. 11 for the four examples shown in Fig. 10. The overall structure of the molecule conformer arises early in the generation process, with

the remainder focused on refinement.

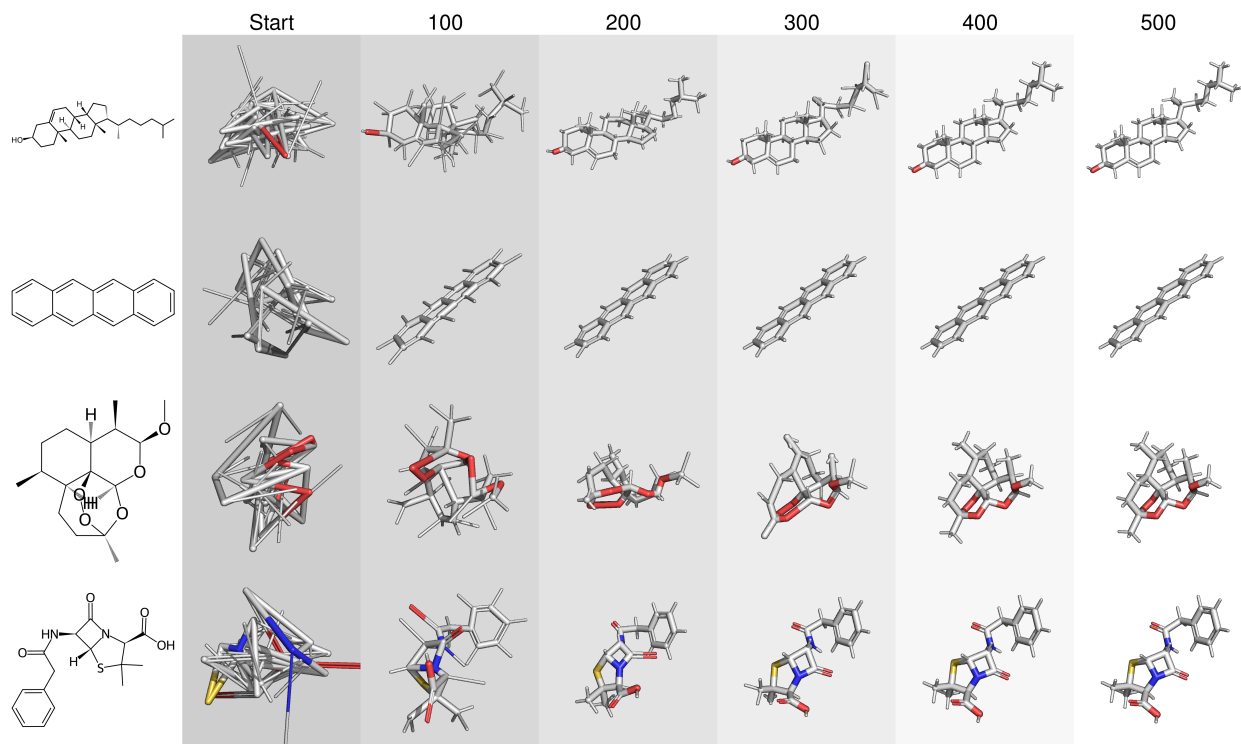


Figure 11: Steps in the generation of the example conformers illustrated in Fig. 10

There are some systems that are challenging to generate. An example is atorvastatin (Fig. 12). This molecule has a central, aromatic ring connected to four large substitutions. This aromatic ring usually fails to generate as flat, probably because planarity imposes tight constraints on the orientation of two of the attached phenyl groups that are difficult to satisfy.

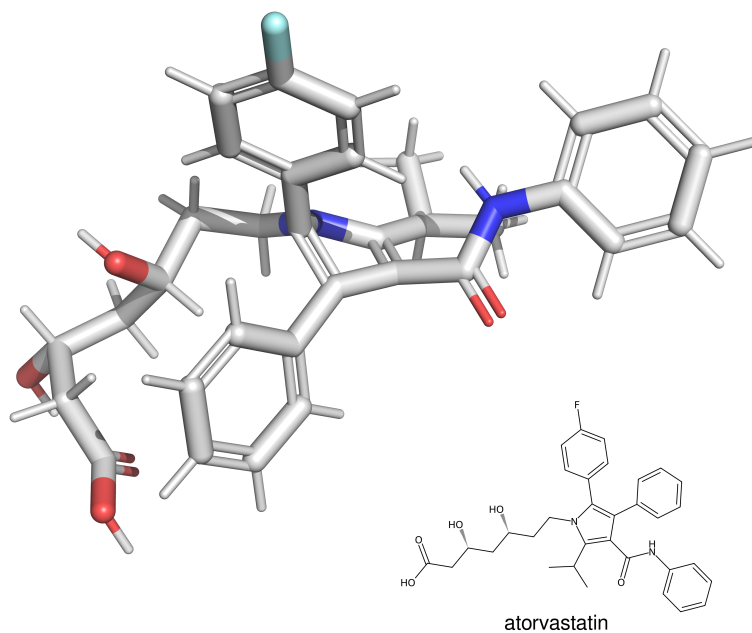


Figure 12: Example of a challenging molecule. Atorvastatin (Lipitor) contains a central, aromatic ring that consistently fails to generate as planar.

Benchmarks

As discussed earlier, 10% of the QMugs data set was set aside as a test subset, corresponding to a random selection of 66,591 molecules. This subset will form the basis for our first set of benchmarks. Because drug molecules are often synthesized as part of a family of closely related compounds during drug development, this randomly selected subset likely contains compounds similar in structure to molecules in the training subset. To remove structural overlap (at the level of the entire molecule) and thus guard against data leakage, Tanimoto similarity is calculated for each molecule against the contents of the QMugs training subset and the entire GEOM-drugs data set. Any molecule with similarity exceeding 0.7 is discarded. The same threshold is also used within the test set to reduce its size and ensure

some level of diversity.

We are interested in reproducing the annotated chirality and cis/trans isomerism of our test compounds. To independently verify this information, each test molecule is checked against the public PubChem database,⁶⁸ and the annotations available there are retrieved for this purpose. In addition, we queried PubChem for a copy of the first 10 of their generated conformers⁶⁹ for later analysis. Molecules that could not be validated or did not have a generated PubChem conformer were discarded.

The final result is an independent set of 15,763 fully annotated test molecules reserved for benchmarks. The molecular weight is an average 15% smaller than the full QMugs data set, but otherwise has a similar shaped distribution.

Although it was not mentioned earlier, the random sample of compounds shown in Fig. 9 were drawn from this independent benchmark set, as are the other examples included in the Supporting Information.

We are interested in establishing conformer accuracy by measuring the reproduction of bonded parameters such as bond length (d), bond angle (θ), and proper torsion angle (ϕ). Proper torsions require special attention because, as discussed earlier, they can have multiple favored values. To limit our statistics to proper torsion angles associated with the same favored angle, we only consider angles that are generated within $\pm 30^\circ$ of the angle found in the reference conformer.

We are also interested in measuring how often a generated structure fails to reproduce the desired chirality and cis/trans isomerism. To do so, we check each related improper torsion and cis/trans bond for a geometry that is consistent with given annotations. Failures are recorded as a fraction of total occurrence of improper torsion atom or cis/trans atom pair.

Because our model makes no attempt to address torsional freedom, the resulting conformers may have atoms that overlap in position (clashes). Although less important for applications which introduce their own torsional sampling (such as flexible ligand docking), clashes nevertheless represent an unphysical molecular state that is explicitly excluded in

conventional conformer generators. To measure their occurrence, we count the fraction of generated conformers that include any nonbonded atom pair within a distance of less than 1.5Å.

To provide overall benchmark statistics, we generate ten random conformers for each of the molecules in the benchmark set. Each generated conformer is compared against all the corresponding conformers for that molecule as provided by QMugs. Overall errors in d , θ , and ϕ (within cutoffs) are measured using the mean absolute deviation (MAD), to avoid sensitivity to tails.

Results are shown in Table 2. In the same table are results taken from other published conformer generation solutions. In all cases, ten conformers are requested, although some conformer solutions by design provide less than the requested number under certain circumstances. Results are briefly summarized below.

Table 2: Benchmark data for the models presented here under various different running conditions and compared against other conformer generation methods. Results for models trained on the QMugs and GEOM-drug data sets are shown for generation steps of size 100, 200 and 500, and using both deterministic and stochastic schemes. Best values in each category are highlighted.

		Mean absolute deviation			Inconsistency rate		Clash rate
		d (Å)	θ (rad)	ϕ (rad)	chirality	cis-trans	< 1.5Å
PIDM[QMugs]							
Deterministic	100	0.0042	0.015	0.036	0.031	0.033	0.753
Deterministic	200	0.0038	0.013	0.027	0.022	0.009	0.681
Deterministic	500	0.0036	0.012	0.023	0.013	0.002	0.576
Stochastic	100	0.0051	0.021	0.079	0.112	0.027	0.587
Stochastic	200	0.0047	0.019	0.069	0.081	0.013	0.571
Stochastic	500	0.0045	0.018	0.062	0.057	0.004	0.549
PIDM[GEOM-drugs]							
Deterministic	100	0.0044	0.015	0.034	0.031	0.034	0.761
Deterministic	200	0.0040	0.013	0.027	0.023	0.015	0.705
Deterministic	500	0.0037	0.012	0.023	0.015	0.005	0.601
Pubchem3D (OMEGA)		0.0075	0.020	0.020	0.020	0.014	0.000
ETKDGv3		0.0183	0.039	0.019	0.000	0.017	0.000
ETKDGv3+MMFF94		0.0081	0.017	0.021	0.000	0.017	0.000
Balloon		0.0082	0.018	0.032	0.002	0.011	0.000
GeoMol		0.0125	0.030	0.042	0.032	0.087	0.495
GeoDiff		0.0051	0.017	0.170	0.500	0.263	0.032

The public PubChem API⁶⁸ provides access to a set of conformers calculated under the PubChem3D scheme.⁶⁹ This scheme is based on the OMEGA toolkit²³ using parameters selected by the authors. Of particular note is the choice to apply the MMFF94s classical forcefield¹³ minus long-distance charged interactions. The results, according to our benchmarks, are robust conformer prediction, particularly for proper torsion angles.

The ETKDGv3^{5,8,24} algorithm produces the most accurate proper torsion values, but is less accurate with bond lengths and angles. Following conformer generation with MMFF94 force field optimization produces conformers of quality similar to PubChem3D, which relies on a similar force field for parameterization. No chirality inconsistencies were detected.

Balloon produces bond distance and bend angle accuracies consistent with other conformer generation solutions that take advantage of the MMFF94 force field.

Like the model presented here, GeoMol focuses on the bonded components of molecules. As mentioned earlier, message passing networks are incapable of detecting cycles,⁵⁵ and so it is not surprising the GeoMol has difficulty accurately representing them, despite incorporating ad-hoc corrections to compensate for this weakness. Tested here is the version of the model trained on the GEOM-drugs data set. Performance is poor by all metrics presented here, especially for bond lengths.

Tested here is the version of GeoDiff³² trained on the GEOM-drugs data set, as provided by the authors. Although this model is capable of accurate bond distance and bend angle prediction, proper torsion angles are poorly reconstructed (Fig. 13). GeoDiff has no mechanism for enforcing chirality nor cis/trans isomerism. Although this limits the usefulness for drug discovery, the omission appears to be an oversight of the authors rather than a fundamental limitation of their approach.

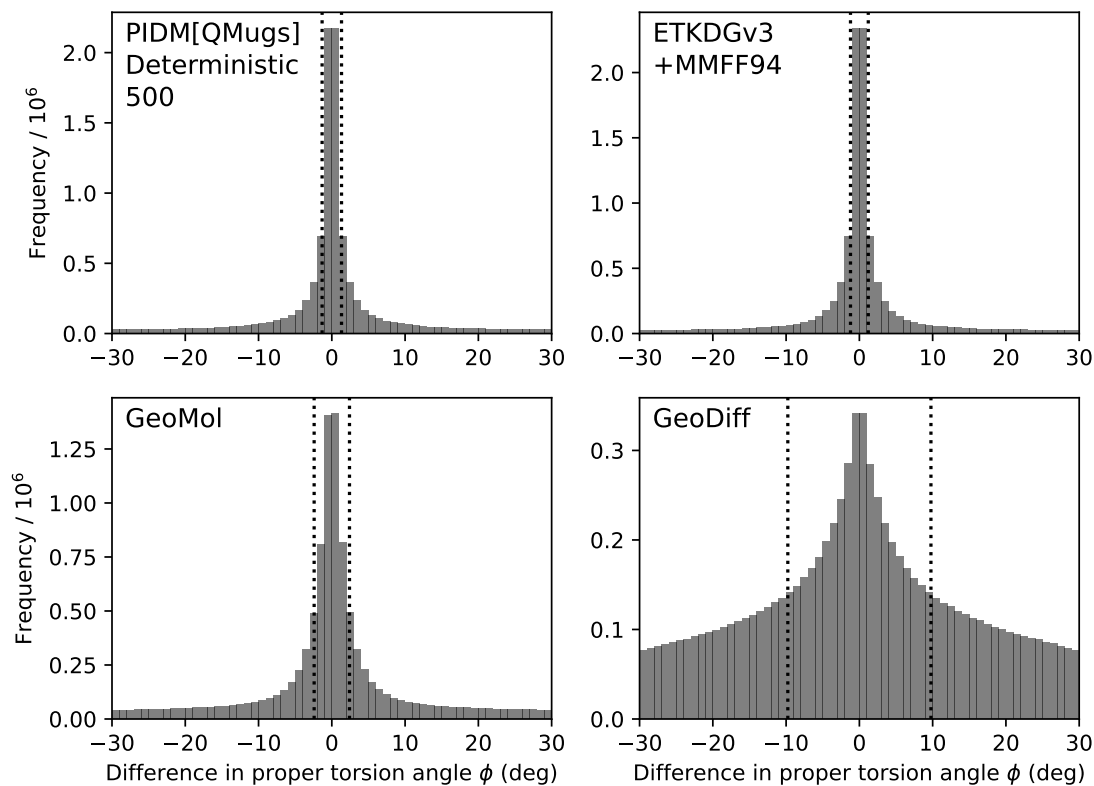


Figure 13: The difference in generated and ground truth for proper torsion angle ϕ for four different generation methods applied to the set of benchmark conformers. The vertical dashed lines indicate the median absolute deviation, calculated for differences with $\pm 30^\circ$.

Several of the conformer methods described above rely on the MMFF94 force field. When compared against benchmark conformers optimized by the more realistic GFN2-xTB semiempirical quantum mechanical method, an overall bias is apparent in bond lengths (Fig. 14). If the bond length parameters in the MMFF94 force field were refit, it's possible that conformer methods such as PubChem3D, RDKit followed by MMFF94, and Balloon would outperform the generative model presented here.

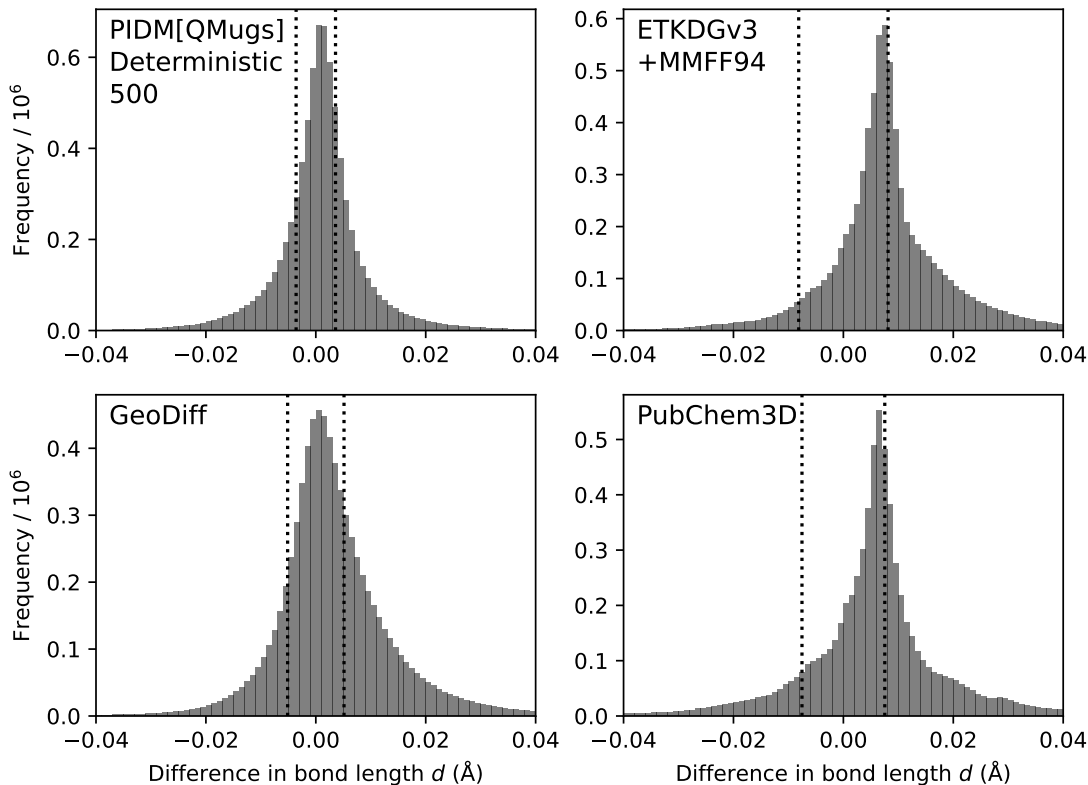


Figure 14: The difference in generated and ground truth for bond distance d for four different generation methods applied to the set of benchmark conformers. The vertical dashed lines indicate the median absolute deviation. The methods in the left column were trained on conformers optimized in the same fashion as the benchmark conformers (GFN2-xTB). The methods in the right column rely on some variation of the MMFF94 force field.

The statistics on ϕ accuracy shown in Table 2 were limited to those cases where the generated proper angle aligned within $\pm 30^\circ$. Accuracy aside, we can check to see how well the overall distribution is reproduced. Interestingly enough, the PIDM models tend to favor $\phi = 0$ more than the conformers provided by QMugs (Fig. 15). The authors of QMugs used an elaborate procedure involving molecular dynamics and clustering via RMSD to select the conformers in their data set, and a uniformity in proper torsion angles is likely a natural consequence of this process.

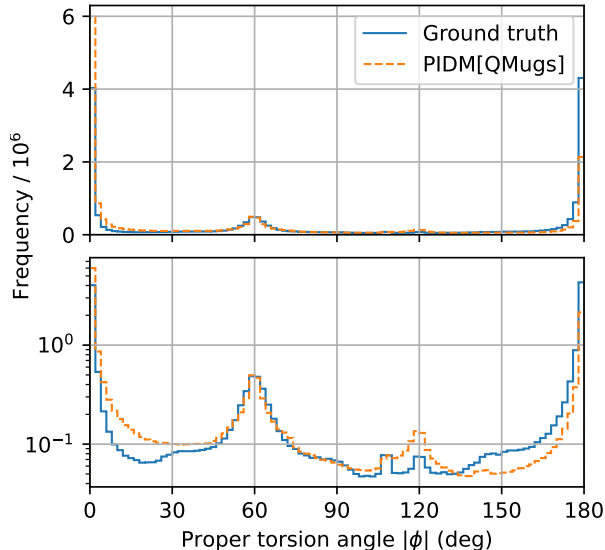


Figure 15: The distribution of the magnitude of proper torsion angle ϕ for the benchmark set of conformers compared to the distribution generated from the same set of molecules using PIDM.

For ligand-protein docking methods that explore torsional freedom during pose optimization, dihedral angle sampling for input conformers should have little relevance. For the benefit of applications that do not independently sample dihedral angles, we can perform further analysis.

The QMugs and GEOM-drugs data sets provide a sample of conformers taken from states of favorable energy calculated in vacuum. These samples are selected to represent some amount of diversity, as measured using the root-mean-squared deviation (RMSD).^{35,57} Although these data sets were constructed with care, they remain synthetic, and the strategies used to enforce diversity somewhat arbitrary. Thus, we see little value in comparing the dihedral sampling of our conformer model to these data sets.

In place of synthetic data sets, we can rely on experimental data. To measure conformer generation performance, the authors of the OMEGA toolkit selected two small experimental sets:²³ 480 molecules from the Cambridge Structural Database (CSD) and 197 ligands from the PDB. We will use the same experimental data here.

Both the CSD and PDB data sets are derived from X-ray data in which only heavy atoms are reliably resolved. The CSD data is for crystalline solids of the molecules either by themselves or with salts. The PDB data set is for ligands bound to proteins. Both are typically resolved in the solid state.

The X-ray structures in the PDB have limited resolution and their solutions are reconstructed, in part, based on assumed force field parameters.⁷⁰ As such, PDB files are not useful for testing the accuracy of bonded parameters. The atom coordinates in the CSD data set, however, are not as constrained by such assumptions. A comparison of the bonded parameters in generated conformers for the CSD data set show the same trends as observed from the QMugs data set, although with lower resolution, presumably due to experimental uncertainties (Table 3). A bias in MMFF94 bond length is confirmed (Fig. 16). Generated results show little bias, presumably reflecting the accuracy (on average) of GFN2-xTB, used in the training data.

Table 3: Statistics on generated conformers compared to experimental data for 480 structures extracted from the CSD. Only bonded terms entirely involving heavy atoms are included.

		Mean absolute deviation			Inconsistency rate		Clash rate < 1.5Å
		d (Å)	θ (rad)	ϕ (rad)	chirality	cis/trans	
PIDM[QMugs]							
Deterministic	500	0.0134	0.030	0.032	0.026	0.003	0.581
Stochastic	500	0.0141	0.035	0.061	0.112	0.016	0.492
PIDM[GEOM-drugs]							
Deterministic	500	0.0136	0.031	0.033	0.039	0.027	0.584
ETKDGv3+MMFF94		0.0161	0.026	0.033	0.000	0.042	0.000
Balloon		0.0163	0.029	0.037	0.000	0.041	0.000
GeoDiff		0.0140	0.030	0.153	0.488	0.242	0.008

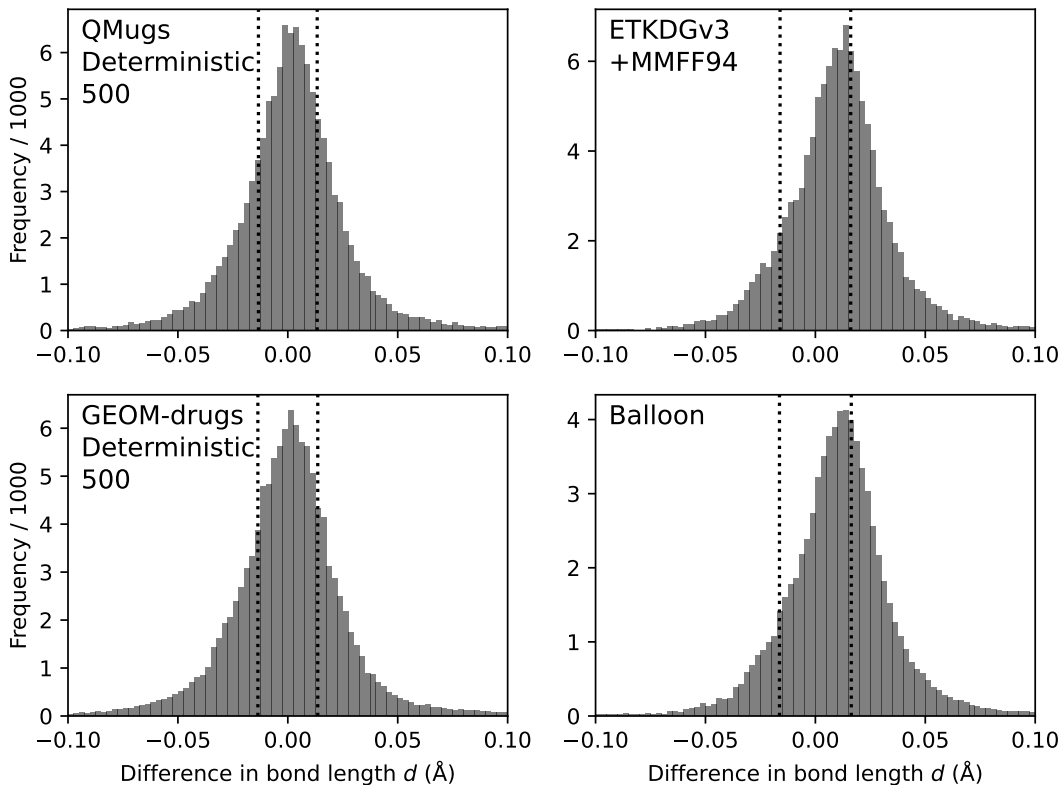


Figure 16: The difference in generated and experimental bond distance d for 480 structures from the CSD. Only bonds involving two heavy atoms are included. The vertical dashed lines indicate the median absolute deviation. Both models on the right rely on some variation of the MMFF94 force field.

We will use the RMSD to measure how well experimental coordinates of the entire molecule are reproduced, calculated on heavy atoms after solid-body alignment. To do so, atoms between generation and experiment are paired by graph matching, where atoms are distinguished by element, formal charge, and number of hydrogens, and bond orders are ignored. The graph matching may produce more than one solution (due to symmetries). The match that produces the smallest RMSD value is used.

Our goal is to use RMSD to measure how close a generator is able to mimic the torsional freedom experimentally observed for a molecule. For our model, in which each conformer is randomly generated, the result will depend on how many attempts we allow. Shown in

Table 4 are statistics for the closest conformer out of 10, 100, and 1,000 attempts. Also shown are published values²³ for the OMEGA toolkit and to 1,000 conformers generated by RDKit followed by MMFF94 optimization. Both OMEGA and RDKit clearly outperform the model presented here, even after 1,000 attempts.

Our model does not consider the distances between nonbonded atom pairs, so it may be unrealistic to expect it to randomly sample torsional angles as effectively as algorithms like OMEGA and ETKDGv3, which are specifically designed to do so. This flaw is evident in the clash rates (Table 3).

Table 4: RMSD statistics on the closest conformer generated through various methods compared to experimental data from the CSD and PDB.

Model	N	RMSD (Å)			
		CSD		PDB	
		Mean	Median	Mean	Median
PIDM[QMugs]	10	1.24	1.38	1.37	1.52
Deterministic 500	100	0.93	1.03	1.04	1.16
	1000	0.74	0.84	0.90	0.98
PIDM[GEOM-drugs]	10	1.28	1.41	1.37	1.59
Deterministic 500	100	0.97	1.10	1.15	1.32
	1000	0.78	0.91	0.96	1.10
OMEGA ^a	—	0.51	0.44	0.67	0.51
RDKit+MMFF94	10	0.70	0.76	0.92	1.06
	100	0.47	0.54	0.67	0.80
	1000	0.43	0.48	0.53	0.64

^a Published statistics²³

To better appreciate the kind of dihedral sample space that our generative model is failing to sample, we can investigate the tail of the RMSD distribution. Shown in Fig. 17 is the ligand from PDB structure 1EC0, which is the molecule with the worst RMSD result (2.9Å). This ligand, a symmetric system with four ring systems, is observed in an extended conformation in the PDB. The best generated pose is more confined. The failure to generate a more compatible, extended conformation could be due to a lack of any explicit mechanism to repel nonbonded atom pairs from each other.

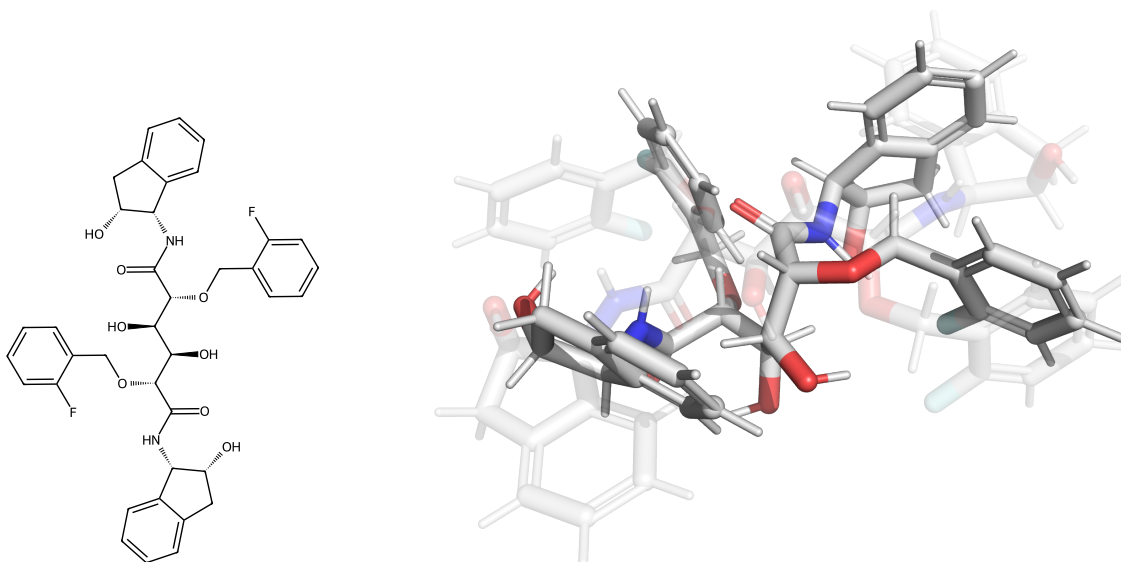


Figure 17: Conformer generation result for the ligand (BEA403) contained in PDB structure 1EC0. The experimental conformer is drawn as transparent. Overlaid is the best RMSD result of 1,000 attempts at generation using PIDM[QMugs].

Guided Generation

As discussed above, our model makes no attempt at predicting the distance between non-bonded pairs of atoms. If we are not concerned about torsional freedom, this is an acceptable compromise. Even so, there are some drawbacks, including the tendency to produce conformers that are more tightly constrained in space than experimentally observed, as discussed in the previous section. The introduction of unphysical clashes may also be an issue, depending on application.

If dihedral sampling is important, some method of introducing bias during generation could be useful. Given that our denoising model places no explicit constraint on the distance between nonbonded atom pairs, one approach for dihedral sampling would be to add some type of bias on that distance during generation. This section describes such an addition as a proof of concept intended to prevent overlapping atoms.

Consider a modified probability flow ODE:

$$\frac{d\mathbf{y}}{dt} = (\mathbf{y} - D(\mathbf{y}; \alpha t) - E(\mathbf{y})) / t, \quad (22)$$

where $E(\mathbf{y})$ is a function external to the denoising model that is introduced in order to guide generation in a desired fashion. Solving for Eq. 22 in place of Eq. 19 provides a mechanism for guided generation where $E(\mathbf{y})$ serves as a type of conditional score.⁴²

For our proof of concept, consider a term that is analogous to a repulsive force of strength δ^{-10} , similar to what is found in the repulsive portion of a Van der Waals interaction:

$$[\Delta_i^n, \Delta_j^n] = -\frac{r_u^{11}}{2} \sum_{ij \in \text{pairs}} \max(\delta_{ij}^2, r_c^2)^{-5} \hat{\delta}_{ij}, \quad (23)$$

where r_c is a clipping distance, nominally set to a value of 0.7\AA , and r_u is a unit distance of 1\AA . Because this term is not trained, it contains no atom embedding and is applied to all nonbonded atom pairs equally. Using Eq. 23, we can introduce a corresponding candidate for $E(\mathbf{y})$ that is moderated by an overall strength η :

$$E(\mathbf{y}) = \eta \sum \Delta^n. \quad (24)$$

Shown in Fig. 18 is the distribution of distances between all atom pairs in the CSD and PDB data sets. Also shown are the same distances sampled from ten conformers generated by PIDM[QMugs] under various conditions and otherwise using 500 steps in the deterministic scheme. With default generation, there is a tendency for atom pairs to overlap, which is unphysical. Adding a term of Eq. 24 with strength $\eta = 0.5$ is sufficient to move the distribution closer to experiment.

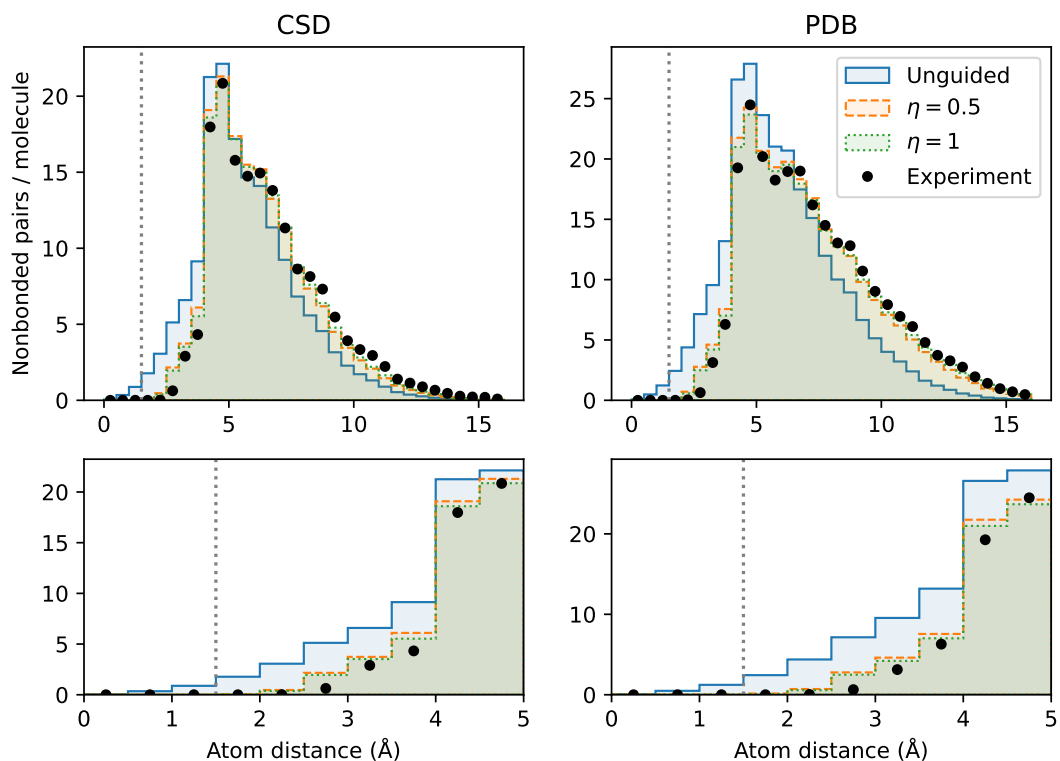


Figure 18: The distribution of distance between all nonbonded atom pairs for the conformers in the CSD and PDB experimental data sets. Also shown are generated results for PIDM[QMugs] using 500 steps in the deterministic scheme. Difference strengths of a repulsive term are applied. The vertical dashed line represents the distance used (1.5\AA) when reporting the clash rate.

The result is a modest improvement in RMSD statistics, as shown in Fig. 19 and Table 5. If we revisit PDB system 1EC0, we observe an improvement in matching the extended conformer observed in that structure (Fig. 20).

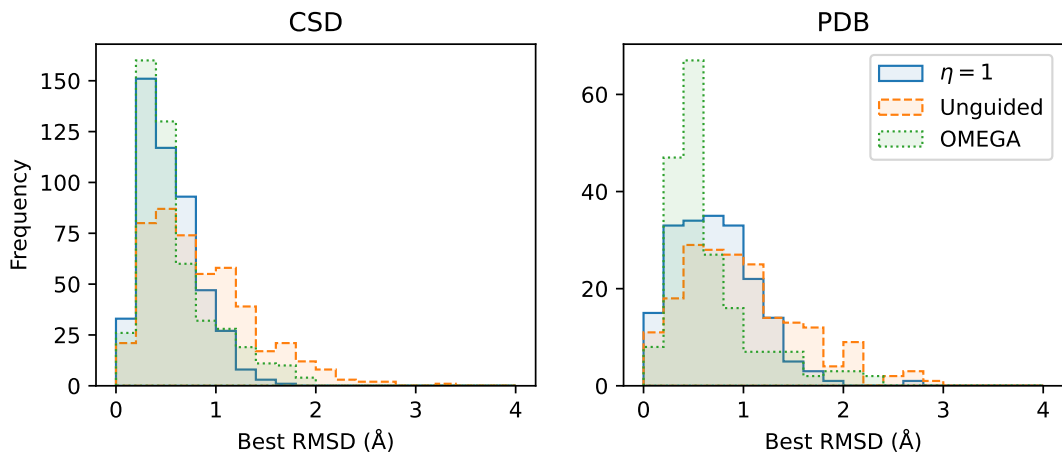


Figure 19: RMSD performance with and without a repulsive term for the CSD and PDB experimental data sets. Shown for comparison are the published results from OMEGA.²³

Table 5: RMSD statistics on the best out of 1,000 conformers generated with and without a repulsion term compared to experimental data from the CSD and PDB. The model shown here is PIDM[QMugs] using the deterministic scheme.

Conditions	RMSD (Å)			
	CSD		PDB	
	Mean	Median	Mean	Median
Undirected	0.74	0.84	0.90	0.98
$\eta = 0.5$	0.53	0.58	0.70	0.75
$\eta = 1$	0.51	0.55	0.67	0.73
OMEGA ^a	0.51	0.44	0.67	0.51

^a Published statistics²³

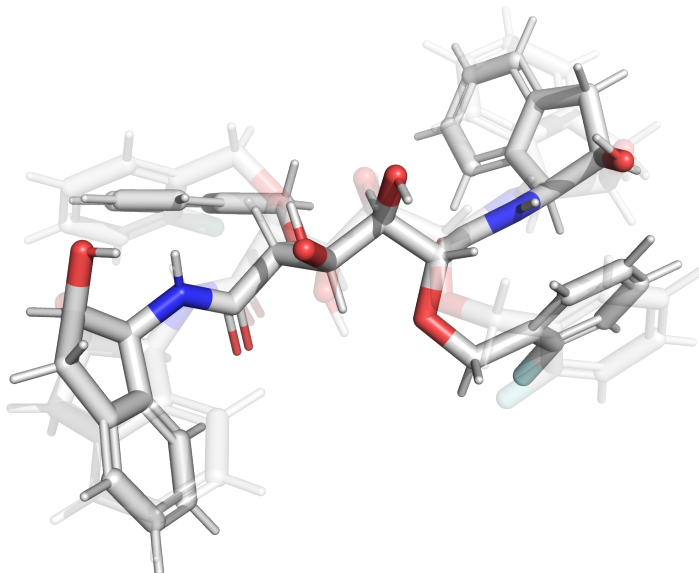


Figure 20: Improved conformer generation result after employing guided generation for the ligand contained in PDB structure 1EC0. The experimenter conformer is presented as transparent. Overlaid is the best RMSD result of 1,000 attempts at generation using PIDM[QMugs] in the deterministic scheme guided by a repulsive strength of $\eta = 1$.

Including a simple repulsive term, however, comes with a cost. As shown in Table 6, error rates for chirality grow to as much as 6%. Fortunately, accuracy in bonded parameters such as bond length d is only marginally affected. Interestingly enough, error rates for cis/trans isomerism actually tend to slightly improve. Clashes are almost entirely eliminated.

Table 6: Bonded benchmark data for our models measured against the benchmark set of 15,763 molecules and generated with and without a repulsive term. Results for models trained on the QMugs and GEOM-drug data sets are shown for 500 steps in the deterministic scheme.

	Mean absolute deviation			Inconsistency rate		Clash rate < 1.5Å
	d (Å)	θ (rad)	ϕ (rad)	chirality	cis/trans	
PIDM[QMugs]						
Unguided	0.0036	0.012	0.023	0.013	0.002	0.576
$\eta = 0.5$	0.0035	0.012	0.025	0.028	0.001	0.000
$\eta = 1$	0.0036	0.012	0.026	0.057	0.001	0.000
PIDM[GEOM-drugs]						
Unguided	0.0037	0.012	0.023	0.015	0.005	0.601
$\eta = 0.5$	0.0036	0.012	0.025	0.029	0.002	0.001
$\eta = 1$	0.0036	0.012	0.025	0.048	0.003	0.000

the CSD and PDB data sets have a relatively small number of proper torsions, and in those cases torsional space can be algorithmically exhausted even with just ten conformers. Note that the RDKit implement of ETKDGv3 provides the option to remove duplicate conformers based on a RMSD threshold, although this option is disabled by default and was not used for the results in this work.

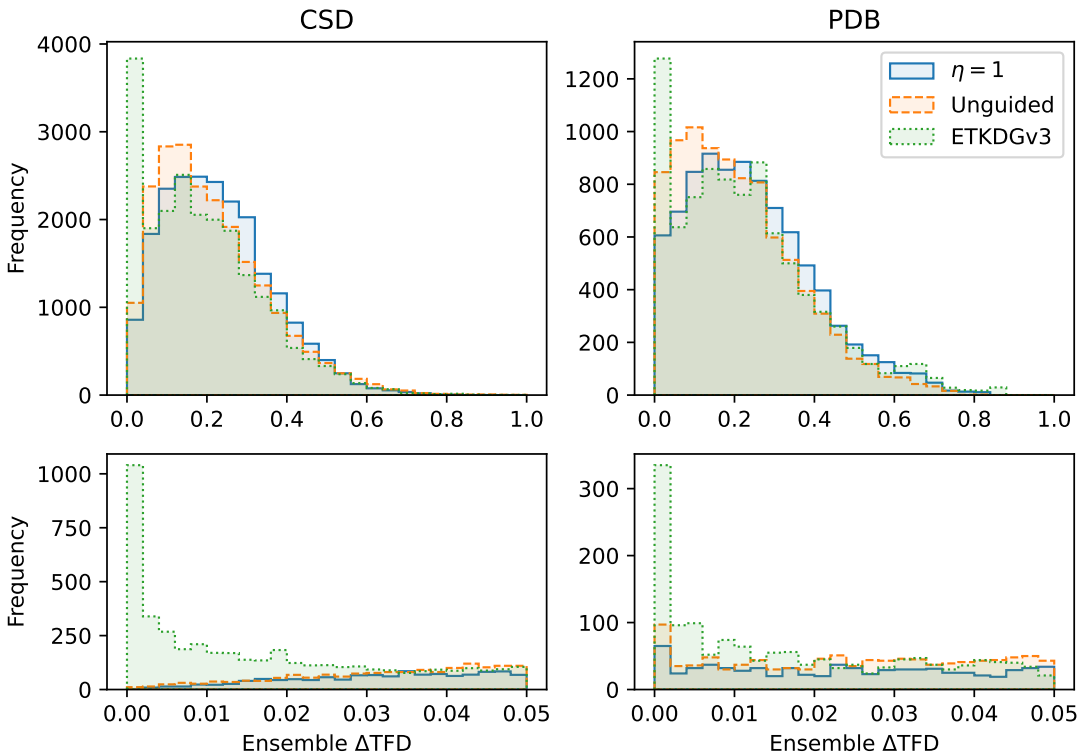


Figure 22: The difference in torsional fingerprint (TFD) values between all pairs of ten conformers generated for the CSD and PDB experimental data sets. Results for PIDM[QMugs] are shown for 500 steps in the deterministic scheme and with or without a repulsive term. Results from RDKit are included for comparison.

Discussion

Conformer generation is an established problem in computational, structure-based drug discovery. Conventional solutions, which have served the community well for decades, are based on carefully tuned, hand-crafted algorithms. Machine learning has made rapid advances re-

cently, and so it is natural to see how well the latest advancements in deep-learning can be applied to this space. One of the goals of this current effort is to remain sensitive to prior work in computational chemistry, particularly in the fields of cheminformatics, classical force fields, and quantum simulation.

In this work, we combine some of the latest advancements in diffusion-based, generative modeling with established techniques used in classical force fields. Classical force fields divide up energy contributions based on subgraph topologies that naturally fit into graph convolution models. They also conveniently divide energy contributions between components that we value (bonded interactions) and those that we deem less important (nonbonded interactions).

Our generative model is based on a denoising model constructed from the sum of five separate, bonded terms. Each term is parameterized by a simple MLP. By training all terms together, the denoising model can account for correlated behavior. Accuracy is improved by ensuring that each term is provided with sufficient information. For example, small rings can influence the angle of any bends they contain. We also find that parameterizing bonded terms as functions of atom distances is more robust than using other geometric measures such as relative angles.

A critique of deep-learning is that the internal structure of a trained model is often inscrutable (they are so-called "black box" models).^{72,73} By constructing our denoising model from the sum of bonded components, we can probe the response of each component separately and explore how the model learned to solve the denoising problem. By using different input molecules as a probe, the solutions for bond lengths, bend angles, and torsion angles can be explored for specific chemical groups. Some examples are presented above, and further are available in the Supporting Information. This ability to test each bonded component under controlled conditions was invaluable during development.

We have used two separate data sets (QMugs and GEOM-drugs) for training. Both include conformers of drug-like molecules optimized in vacuum using GFN2-xTB, a semiem-

pirical quantum mechanical calculation. This type of calculation is expected to provide bonded parameters more accurate than available from classical force fields. During training, the losses calculated on holdout validation data sets show no evidence of increasing, suggesting little overtraining. This loss also matches the loss from the training subset, implying a level of transferability. Remarkably, despite little overlap in the two training sets, the resulting models perform nearly identically on all benchmarks. Probes indicate that both models have learned similar solutions.

For generation, we numerically solve for the probability flow ODE, using a form of oversampling. Both deterministic and stochastic generation are tested, and the former outperforms the latter for most criteria. Generation in as little as 100 steps appears sufficient for conformers of reasonable quality, but using more steps noticeably improves performance.

To test the accuracy of generated conformers, we use an independent subset of the QMugs data set. We used Tanimoto similarity to ensure the molecules in this subset had little structural overlap with the training subsets. Based on the median absolute deviation, generated conformers have more accurate bond lengths and bond angles than established solutions, at least on average. Much of the reason is likely due to training on structures optimized by GFN2-xTB, whereas established conformer solutions rely, in part, on force field parameterization, such as MMFF94.

Average performance on proper torsion angle is also competitive. It is interesting that another published diffusion model, GeoDiff, performs quite poorly on torsional angles. GeoDiff also requires ten times the amount of generation steps and contains about six times as many parameters.

Molecule conformers for drug-like compounds typically achieve a large part of their diversity from torsional freedom. Outside of macrocycles, dihedral angles are relatively easy to manipulate, which is why they are among the degrees of freedom commonly optimized in ligand-protein docking algorithms. In such applications, the focus of a conformer generator should be the production of quality bonded parameters, such as bond lengths, bend angles,

and ring conformations.

Conformer RMSD is sensitive to dihedral angles. This makes the RMSD a poor metric for evaluating the quality of generated conformers, unless the goal is to reproduce the selection of dihedral angles. Gauging the quality of a conformer generator based on reproducing the RMSD of synthetic data sets, such as QMugs and GEOM-drugs, is merely testing if the generator can reproduce the somewhat arbitrary choices the authors of these data sets employed for dihedral angle sampling.

Measuring RMSD against experimental data does have value, but data is limited in size and resolution and restricted to certain physical conditions, such as crystal solids. For training, limited statistics is a problem for deep-learning techniques which rely on a large and diverse sample of training data.

We used experimental data to explore the dihedral space sampled by our conformer generation model and have uncovered some deficiencies. This is a problem for applications that do not independently sample dihedral space. This deficiency can be partially mitigated by introducing a form of guided generation. We tested a simple technique that applied a universal repulsion between nonbonded atom pairs. One could imagine more complex guided techniques that are capable of sampling dihedral angles appropriate for any number of molecule environments or conditions.

The atom encoding used in our model was generated using a Graph Attention Transformer (GATv2).⁵³ One could substitute other types of comparable message-passing graph networks, such as a Graph Isomorphism Network (GIN),⁷⁴ and probably obtain comparable results. We suspect that using a type of graph network that can capture the same quality of chemical information while also recognizing cycles would be an improvement. Such a graph model would not only allow the removal of the ad-hoc ring embedding we use for the bend angle component, but also provide a mechanism for correcting bond lengths and torsion angles that are also impacted by rings.

Other challenges remain. There are some molecules that fail to generate correctly, such as

atorvastatin. Because our denoising model is based on local molecular structure (via bonded components), large scale movements, such as those needed to swing an arm of a molecule to ensure planarity for an aromatic ring, are difficult to accommodate.

On average, the generative model presented here reproduces bonded parameters with an accuracy comparable to conventional methods (such as OMEGA and ETKDGv3), with perhaps the exception of dihedral angle sampling. This is accomplished without relying on preestablished constraints, template libraries, or external parameterizations such as classical force fields. Extending this model to additional atom types should only require the construction of a suitably representative molecule data set for training that can be prepared using GFN2-xTB. It should also be possible to employ masking techniques, widely available for images,⁷⁵⁻⁷⁷ to extend molecule conformer generation to tasks such as fragment bridging⁷⁸⁻⁸⁰ and fragment screening.^{81,82}

Conclusion

Presented is a physics-inspired, diffusion-based model for molecule conformer generation inspired by the bonded components of classical force fields. Parameters were trained on high-quality conformers from the QMugs and GEOM-drugs data sets. Learning appears robust, transferable, and explainable. Both deterministic and stochastic generation schemes are demonstrated. Average performance on the reproduction of bonded parameters exceeds conventional conformer generation tools. A simple example of guided generation is successful at improving dihedral sampling when compared to experimental data.

Data and Software Availability

A complete model implementation is available in source form at <https://github.com/nobiastx/diffusion-conformer>. Included are model checkpoints and scripts for training and inference. The training and benchmark data (QMugs, GEOM-drugs, CSD, and PDB) are available from public

sources.

Supporting Information Available

The following files are available free of charge:

- Figs. S1–S17, additional model probes, Figs. S18–S23, additional example conformer output.
- Video of example generation of cholesterol, using PIDM[QMugs] and 500 steps in the deterministic scheme.
- Video of example generation of naphthacene, same conditions.
- Video of example generation of artemether, same conditions.
- Video of example generation of penicillin, same conditions.
- Molecular structure file containing the conformer output for Fig. 9 from the main text and Figs. S18–S23 from the Supporting Information.

References

- (1) Schaduangrat, N.; Lampa, S.; Simeon, S.; Gleeson, M. P.; Spjuth, O.; Nantasenamat, C. Towards reproducible computational drug discovery. *Journal of Cheminformatics* **2020**, *12*, 9.
- (2) Gasteiger, J.; Rudolph, C.; Sadowski, J. Automatic generation of 3D-atomic coordinates for organic molecules. *Tetrahedron Computer Methodology* **1990**, *3*, 537–547.
- (3) Vainio, M. J.; Johnson, M. S. Generating Conformer Ensembles Using a Multiobjective Genetic Algorithm. *Journal of Chemical Information and Modeling* **2007**, *47*, 2462–2474.

- (4) Corbeil, C. R.; Moitessier, N. Docking Ligands into Flexible and Solvated Macromolecules. 3. Impact of Input Ligand Conformation, Protein Flexibility, and Water Molecules on the Accuracy of Docking Programs. *Journal of Chemical Information and Modeling* **2009**, *49*, 997–1009, Publisher: American Chemical Society.
- (5) Riniker, S.; Landrum, G. A. Better Informed Distance Geometry: Using What We Know To Improve Conformation Generation. *Journal of Chemical Information and Modeling* **2015**, *55*, 2562–2574, Publisher: American Chemical Society.
- (6) Hawkins, P. C. D. Conformation Generation: The State of the Art. *Journal of Chemical Information and Modeling* **2017**, *57*, 1747–1756, Publisher: American Chemical Society.
- (7) Friedrich, N.-O.; de Bruyn Kops, C.; Flachsenberg, F.; Sommer, K.; Rarey, M.; Kirchmair, J. Benchmarking Commercial Conformer Ensemble Generators. *Journal of Chemical Information and Modeling* **2017**, *57*, 2719–2728, Publisher: American Chemical Society.
- (8) Wang, S.; Witek, J.; Landrum, G. A.; Riniker, S. Improving Conformer Generation for Small Rings and Macrocycles Based on Distance Geometry and Experimental Torsional-Angle Preferences. *Journal of Chemical Information and Modeling* **2020**, *60*, 2044–2058, Publisher: American Chemical Society.
- (9) Leite, T. B.; Gomes, D.; Miteva, M.; Chomilier, J.; Villoutreix, B.; Tufféry, P. Frog: a FRee Online druG 3D conformation generator. *Nucleic Acids Research* **2007**, *35*, W568–W572.
- (10) Lagorce, D.; Pencheva, T.; Villoutreix, B. O.; Miteva, M. A. DG-AMMOS: A New tool to generate 3D conformation of small molecules using Distance Geometry and Automated Molecular Mechanics Optimization for in silico Screening. *BMC Chemical Biology* **2009**, *9*, 6.

- (11) Dauber-Osguthorpe, P.; Hagler, A. T. Biomolecular force fields: where have we been, where are we now, where do we need to go and how do we get there? *Journal of Computer-Aided Molecular Design* **2019**, *33*, 133–203.
- (12) Case, D. A.; Cheatham III, T. E.; Darden, T.; Gohlke, H.; Luo, R.; Merz Jr., K. M.; Onufriev, A.; Simmerling, C.; Wang, B.; Woods, R. J. The Amber biomolecular simulation programs. *Journal of Computational Chemistry* **2005**, *26*, 1668–1688, _eprint: <https://onlinelibrary.wiley.com/doi/pdf/10.1002/jcc.20290>.
- (13) Halgren, T. A. Merck molecular force field. I. Basis, form, scope, parameterization, and performance of MMFF94. *Journal of Computational Chemistry* **1996**, *17*, 490–519.
- (14) Guo, L.; Yan, Z.; Zheng, X.; Hu, L.; Yang, Y.; Wang, J. A comparison of various optimization algorithms of protein-ligand docking programs by fitness accuracy. *Journal of Molecular Modeling* **2014**, *20*.
- (15) Kitchen, D. B.; Decornez, H.; Furr, J. R.; Bajorath, J. Docking and scoring in virtual screening for drug discovery: methods and applications. *Nature Reviews Drug Discovery* **2004**, *3*, 935–949.
- (16) Pagadala, N. S.; Syed, K.; Tuszynski, J. Software for molecular docking: a review. *Biophysical Reviews* **2017**, *9*, 91–102.
- (17) Corso, G.; Stärk, H.; Jing, B.; Barzilay, R.; Jaakkola, T. DiffDock: Diffusion Steps, Twists, and Turns for Molecular Docking. 2022; <http://arxiv.org/abs/2210.01776>, arXiv:2210.01776 [physics, q-bio].
- (18) Nelson, D. J.; Brammer, C. N. Toward Consistent Terminology for Cyclohexane Conformers in Introductory Organic Chemistry. *Journal of Chemical Education* **2011**, *88*, 292–294, Publisher: American Chemical Society.

- (19) Jamali, F.; Mehvar, R.; Pasutto, F. M. Enantioselective Aspects of Drug Action and Disposition: Therapeutic Pitfalls. *Journal of Pharmaceutical Sciences* **1989**, *78*, 695–715.
- (20) Brooks, W.; Guida, W.; Daniel, K. The Significance of Chirality in Drug Design and Development. *Current topics in medicinal chemistry* **2011**, *11*, 760–770.
- (21) Dugave, C.; Demange, L. Cis- trans isomerization of organic molecules and biomolecules: implications and applications. *Chemical reviews* **2003**, *103*, 2475–2532.
- (22) Chastine, J. W.; Brooks, J. C.; Zhu, Y.; Owen, G. S.; Harrison, R. W.; Weber, I. T. Ammp-vis: a collaborative virtual environment for molecular modeling. Proceedings of the ACM symposium on Virtual reality software and technology. 2005; pp 8–15.
- (23) Hawkins, P. C. D.; Skillman, A. G.; Warren, G. L.; Ellingson, B. A.; Stahl, M. T. Conformer Generation with OMEGA: Algorithm and Validation Using High Quality Structures from the Protein Databank and Cambridge Structural Database. *Journal of Chemical Information and Modeling* **2010**, *50*, 572–584, Publisher: American Chemical Society.
- (24) Landrum, G. et al. RDKit: Open-source cheminformatics. 2021; <https://doi.org/10.5281/zenodo.7235579>, [10.5281/zenodo.3732262](https://doi.org/10.5281/zenodo.3732262).
- (25) Luo, S.; Shi, C.; Xu, M.; Tang, J. Predicting Molecular Conformation via Dynamic Graph Score Matching. *Advances in Neural Information Processing Systems*. 2021; pp 19784–19795.
- (26) Shi, C.; Luo, S.; Xu, M.; Tang, J. Learning Gradient Fields for Molecular Conformation Generation. *Proceedings of the 38th International Conference on Machine Learning*. 2021; pp 9558–9568, ISSN: 2640-3498.

- (27) Xu, M.; Luo, S.; Bengio, Y.; Peng, J.; Tang, J. Learning Neural Generative Dynamics for Molecular Conformation Generation. 2021; <http://arxiv.org/abs/2102.10240>, arXiv:2102.10240 [physics].
- (28) Mansimov, E.; Mahmood, O.; Kang, S.; Cho, K. Molecular Geometry Prediction using a Deep Generative Graph Neural Network. *Scientific Reports* **2019**, *9*, 20381, Number: 1 Publisher: Nature Publishing Group.
- (29) Simm, G. N. C.; Hernández-Lobato, J. M. A Generative Model for Molecular Distance Geometry. 2020; <http://arxiv.org/abs/1909.11459>, arXiv:1909.11459 [cs, stat].
- (30) Xu, M.; Wang, W.; Luo, S.; Shi, C.; Bengio, Y.; Gomez-Bombarelli, R.; Tang, J. An End-to-End Framework for Molecular Conformation Generation via Bilevel Programming. Proceedings of the 38th International Conference on Machine Learning. 2021; pp 11537–11547, ISSN: 2640-3498.
- (31) Ganea, O.; Pattanaik, L.; Coley, C.; Barzilay, R.; Jensen, K.; Green, W.; Jaakkola, T. GeoMol: Torsional Geometric Generation of Molecular 3D Conformer Ensembles. Advances in Neural Information Processing Systems. 2021; pp 13757–13769.
- (32) Xu, M.; Yu, L.; Song, Y.; Shi, C.; Ermon, S.; Tang, J. GeoDiff: a Geometric Diffusion Model for Molecular Conformation Generation. 2022; <http://arxiv.org/abs/2203.02923>, Number: arXiv:2203.02923 arXiv:2203.02923 [cs, q-bio].
- (33) Ho, J.; Jain, A.; Abbeel, P. Denoising Diffusion Probabilistic Models. **2020**,
- (34) Jing, B.; Corso, G.; Chang, J.; Barzilay, R.; Jaakkola, T. Torsional Diffusion for Molecular Conformer Generation. *Advances in Neural Information Processing Systems* **2022**, *35*, 24240–24253.
- (35) Axelrod, S.; Gómez-Bombarelli, R. GEOM, energy-annotated molecular conformations

for property prediction and molecular generation. *Scientific Data* **2022**, *9*, 185, Number: 1 Publisher: Nature Publishing Group.

- (36) Sohl-Dickstein, J.; Weiss, E. A.; Maheswaranathan, N.; Ganguli, S. Deep Unsupervised Learning using Nonequilibrium Thermodynamics. 2015; <http://arxiv.org/abs/1503.03585>, Number: arXiv:1503.03585 arXiv:1503.03585 [cond-mat, q-bio, stat].
- (37) Croitoru, F.-A.; Hondru, V.; Ionescu, R. T.; Shah, M. Diffusion Models in Vision: A Survey. *IEEE Transactions on Pattern Analysis and Machine Intelligence* **2023**, *45*, 10850–10869, Conference Name: IEEE Transactions on Pattern Analysis and Machine Intelligence.
- (38) DALL-E. 2023; <https://en.wikipedia.org/w/index.php?title=DALL-E&oldid=1171382222>, Page Version ID: 1171382222.
- (39) Midjourney. 2023; <https://en.wikipedia.org/w/index.php?title=Midjourney&oldid=1173734882>, Page Version ID: 1173734882.
- (40) Schaul, K.; Shaban, H.; Tan, S.; Woo, M.; Tiku, N. AI can now create images out of thin air. See how it works. <https://www.washingtonpost.com/technology/interactive/2022/ai-image-generator/>.
- (41) Karras, T.; Aittala, M.; Aila, T.; Laine, S. Elucidating the Design Space of Diffusion-Based Generative Models. *Advances in Neural Information Processing Systems*. 2022.
- (42) Luo, C. Understanding Diffusion Models: A Unified Perspective. 2022; <http://arxiv.org/abs/2208.11970>, arXiv:2208.11970 [cs].
- (43) Nichol, A. Q.; Dhariwal, P. Improved Denoising Diffusion Probabilistic Models. *Proceedings of the 38th International Conference on Machine Learning*. 2021; pp 8162–8171, ISSN: 2640-3498.

- (44) Kingma, D.; Salimans, T.; Poole, B.; Ho, J. Variational Diffusion Models. *Advances in Neural Information Processing Systems*. 2021; pp 21696–21707.
- (45) Song, Y.; Sohl-Dickstein, J.; Kingma, D. P.; Kumar, A.; Ermon, S.; Poole, B. Score-Based Generative Modeling through Stochastic Differential Equations. 2022.
- (46) Luo, S.; Hu, W. Diffusion Probabilistic Models for 3D Point Cloud Generation. 2021; pp 2837–2845.
- (47) Kong, Z.; Ping, W.; Huang, J.; Zhao, K.; Catanzaro, B. DiffWave: A Versatile Diffusion Model for Audio Synthesis. 2021.
- (48) Daniels, M.; Maunu, T.; Hand, P. Score-based Generative Neural Networks for Large-Scale Optimal Transport. 2022.
- (49) Chen, K.; Chen, X.; Yu, Z.; Zhu, M.; Yang, H. EquiDiff: A Conditional Equivariant Diffusion Model For Trajectory Prediction. 2023.
- (50) Wang, W.; Yang, D.; Ye, Q.; Cao, B.; Zou, Y. NADiffuSE: Noise-aware Diffusion-based Model for Speech Enhancement. 2023.
- (51) Rombach, R.; Blattmann, A.; Lorenz, D.; Esser, P.; Ommer, B. High-Resolution Image Synthesis With Latent Diffusion Models. 2022; pp 10684–10695.
- (52) Vincent, P. A Connection Between Score Matching and Denoising Autoencoders. *Neural Computation* **2011**, *23*, 1661–1674, Conference Name: Neural Computation.
- (53) Brody, S.; Alon, U.; Yahav, E. How Attentive are Graph Attention Networks? *arXiv:2105.14491 [cs]* **2022**, arXiv: 2105.14491.
- (54) Glendening, E. D.; Weinhold, F. Natural resonance theory: II. Natural bond order and valency. *Journal of Computational Chemistry* **1998**, *19*, 610–627.

- (55) Xu, K.; Hu, W.; Leskovec, J.; Jegelka, S. *How Powerful are Graph Neural Networks?*; 2019; arXiv:1810.00826 [cs, stat] type: article.
- (56) Loshchilov, I.; Hutter, F. Decoupled Weight Decay Regularization. 2017; <https://arxiv.org/abs/1711.05101v3>.
- (57) Isert, C.; Atz, K.; Jiménez-Luna, J.; Schneider, G. QMugs, quantum mechanical properties of drug-like molecules. *Scientific Data* **2022**, *9*, 273, Number: 1 Publisher: Nature Publishing Group.
- (58) Grimme, S.; Bannwarth, C.; Shushkov, P. A Robust and Accurate Tight-Binding Quantum Chemical Method for Structures, Vibrational Frequencies, and Noncovalent Interactions of Large Molecular Systems Parametrized for All spd-Block Elements ($Z = 1-86$). *Journal of Chemical Theory and Computation* **2017**, *13*, 1989–2009, Publisher: American Chemical Society.
- (59) Bannwarth, C.; Ehlert, S.; Grimme, S. GFN2-xTB—An Accurate and Broadly Parametrized Self-Consistent Tight-Binding Quantum Chemical Method with Multipole Electrostatics and Density-Dependent Dispersion Contributions. *Journal of Chemical Theory and Computation* **2019**, *15*, 1652–1671, Publisher: American Chemical Society.
- (60) Wildman, S. A.; Crippen, G. M. Prediction of Physicochemical Parameters by Atomic Contributions. *Journal of Chemical Information and Computer Sciences* **1999**, *39*, 868–873, Publisher: American Chemical Society.
- (61) Mendez, D. et al. ChEMBL: towards direct deposition of bioassay data. *Nucleic Acids Research* **2019**, *47*, D930–D940.
- (62) MIT Schwarzman College of Computing, I. AI Cures: data-driven clinical solutions for Covid-19. 2020; <https://www.aicures.mit.edu/data>.

- (63) Yang, K. Data and scripts for COVID-19. https://github.com/yangkevin2/coronavirus_data, 2020.
- (64) Wu, Z.; Ramsundar, B.; E.N. Feinberg, E.; Gomes, J.; Geniesse, C.; A.S. Pappu, A.; Leswing, K.; Pande, V. MoleculeNet: a benchmark for molecular machine learning. *Chemical Science* **2018**, *9*, 513–530, Publisher: Royal Society of Chemistry.
- (65) Song, J.; Meng, C.; Ermon, S. Denoising Diffusion Implicit Models. 2022; <http://arxiv.org/abs/2010.02502>, arXiv:2010.02502 [cs].
- (66) Bansal, A.; Borgnia, E.; Chu, H.-M.; Li, J. S.; Kazemi, H.; Huang, F.; Goldblum, M.; Geiping, J.; Goldstein, T. Cold Diffusion: Inverting Arbitrary Image Transforms Without Noise. 2022; <http://arxiv.org/abs/2208.09392>, arXiv:2208.09392 [cs].
- (67) Song, Y.; Dhariwal, P.; Chen, M.; Sutskever, I. Consistency Models. 2023; <http://arxiv.org/abs/2303.01469>, arXiv:2303.01469 [cs, stat].
- (68) Kim, S.; Chen, J.; Cheng, T.; Gindulyte, A.; He, J.; He, S.; Li, Q.; Shoemaker, B. A.; Thiessen, P. A.; Yu, B., et al. PubChem 2023 update. *Nucleic Acids Research* **2023**, *51*, D1373–D1380.
- (69) Bolton, E. E.; Kim, S.; Bryant, S. H. PubChem3D: Conformer generation. *Journal of Cheminformatics* **2011**, *3*, 4.
- (70) Deller, M. C.; Rupp, B. Models of protein-ligand crystal structures: trust, but verify. *Journal of computer-aided molecular design* **2015**, *29*, 817–836.
- (71) Schulz-Gasch, T.; Schärfer, C.; Guba, W.; Rarey, M. TFD: Torsion Fingerprints As a New Measure To Compare Small Molecule Conformations. *Journal of Chemical Information and Modeling* **2012**, *52*, 1499–1512, Publisher: American Chemical Society.
- (72) Rudin, C. Stop explaining black box machine learning models for high stakes decisions

- and use interpretable models instead. *Nature Machine Intelligence* **2019**, *1*, 206–215, Number: 5 Publisher: Nature Publishing Group.
- (73) Blazek, P. J.; Lin, M. M. Explainable neural networks that simulate reasoning. *Nature Computational Science* **2021**, *1*, 607–618, Number: 9 Publisher: Nature Publishing Group.
- (74) Xu, K.; Hu, W.; Leskovec, J.; Jegelka, S. How powerful are graph neural networks? *arXiv preprint arXiv:1810.00826* **2018**,
- (75) Liu, H.; Jiang, B.; Song, Y.; Huang, W.; Yang, C. Rethinking image inpainting via a mutual encoder-decoder with feature equalizations. *Computer Vision–ECCV 2020: 16th European Conference, Glasgow, UK, August 23–28, 2020, Proceedings, Part II* 16. 2020; pp 725–741.
- (76) Lugmayr, A.; Danelljan, M.; Romero, A.; Yu, F.; Timofte, R.; Van Gool, L. RePaint: Inpainting Using Denoising Diffusion Probabilistic Models. 2022; pp 11461–11471.
- (77) Kirillov, A.; Mintun, E.; Ravi, N.; Mao, H.; Rolland, C.; Gustafson, L.; Xiao, T.; Whitehead, S.; Berg, A. C.; Lo, W.-Y.; Dollár, P.; Girshick, R. Segment Anything. 2023; <http://arxiv.org/abs/2304.02643>, arXiv:2304.02643 [cs].
- (78) Lauri, G.; Bartlett, P. A. CAVEAT: A program to facilitate the design of organic molecules. *Journal of Computer-Aided Molecular Design* **1994**, *8*, 51–66.
- (79) Thompson, D. C.; Aldrin Denny, R.; Nilakantan, R.; Humblet, C.; Joseph-McCarthy, D.; Feyfant, E. CONFIRM: connecting fragments found in receptor molecules. *Journal of Computer-Aided Molecular Design* **2008**, *22*, 761–772.
- (80) Imrie, F.; Bradley, A. R.; van der Schaar, M.; Deane, C. M. Deep Generative Models for 3D Linker Design. *Journal of Chemical Information and Modeling* **2020**, *60*, 1983–1995, Publisher: American Chemical Society.

- (81) Kumar, A.; Voet, A.; Zhang, K. Fragment Based Drug Design: From Experimental to Computational Approaches. *Current Medicinal Chemistry* **2012**, *19*, 5128–5147.
- (82) Jacquemard, C.; Kellenberger, E. A bright future for fragment-based drug discovery: what does it hold? *Expert Opinion on Drug Discovery* **2019**, *14*, 413–416, Publisher: Taylor & Francis _eprint: <https://doi.org/10.1080/17460441.2019.1583643>.

Supporting Information

Additional model probes

The bonded components of any molecule can be explored. The following are selected as representative. It is also informative to compare PIDM[QMugs] and PIDM[GEOM-drugs]. Interested readers are encouraged to perform their own experiments and source code is provided for this purpose.

Each of the figures below include four plots arranged in a grid. The left (right) column is reserved for PIDM[QMugs] (PIDM[GEOM-drugs]). Each row corresponds to one of a pair of atoms for the bond, bend, proper torsion, and chirality probes, or a pair of atoms for the cis-trans probe. The identity of the atoms are highlighted by the circle(s) in the molecule depiction on the left.

Each plot includes corrections for various values of σ . The vertical gray line is the expected value, from a GFN2-xTB optimization.

Bond component

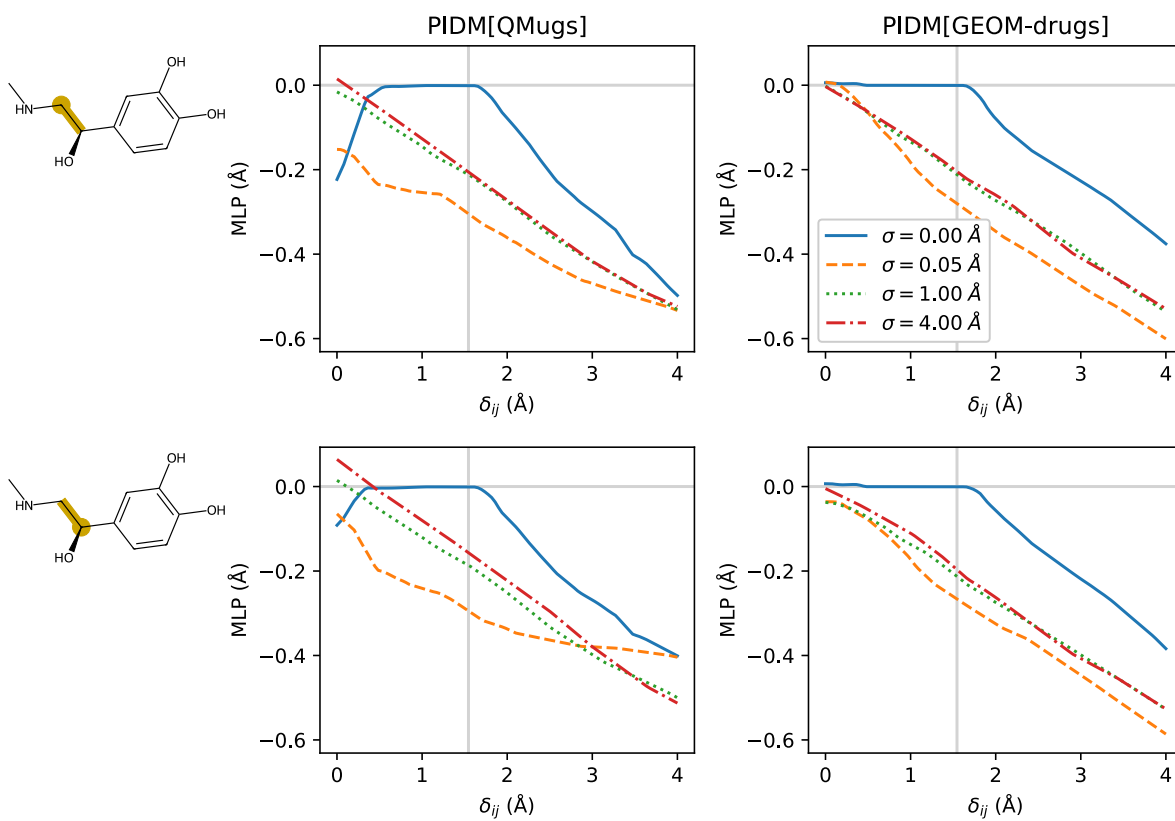


Figure 23: Example bond correction for the two atoms involved in an alkane bond in adrenaline.

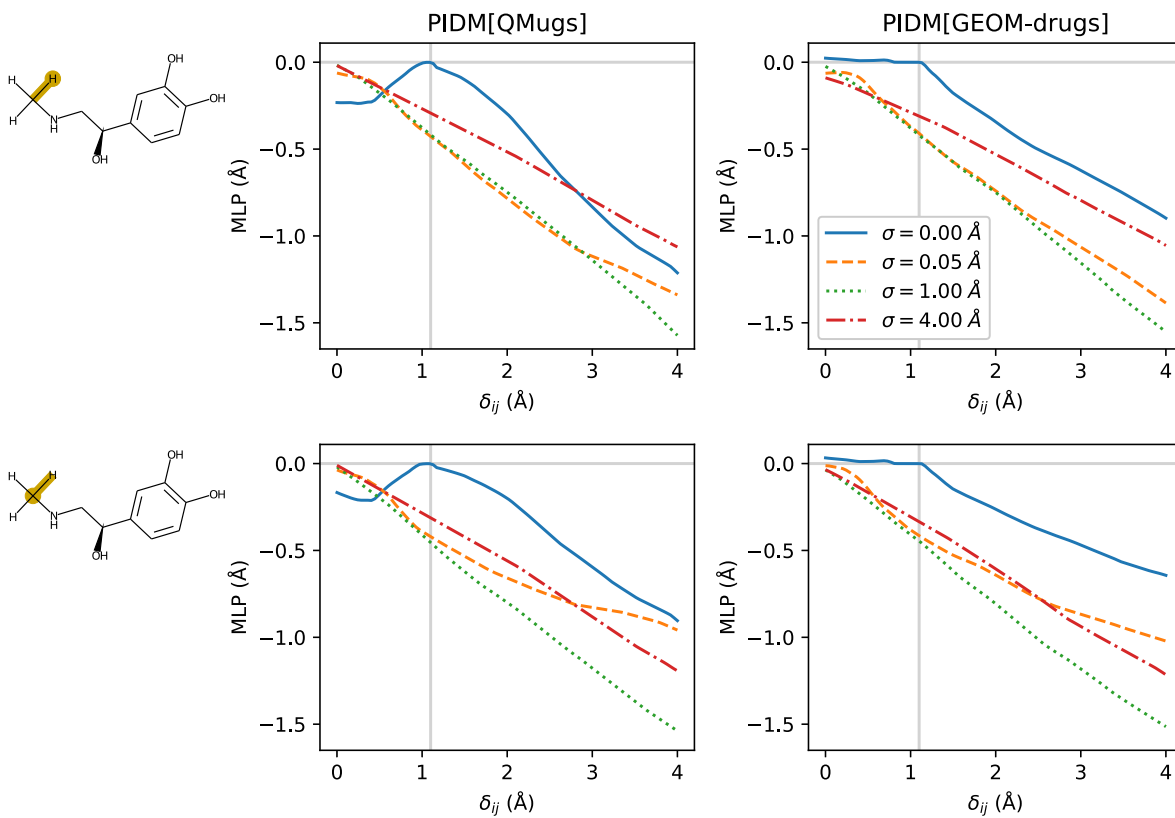


Figure 24: Example bond correction for one of the hydrogens (top row) on a primary carbon (bottom row) in adrenaline.

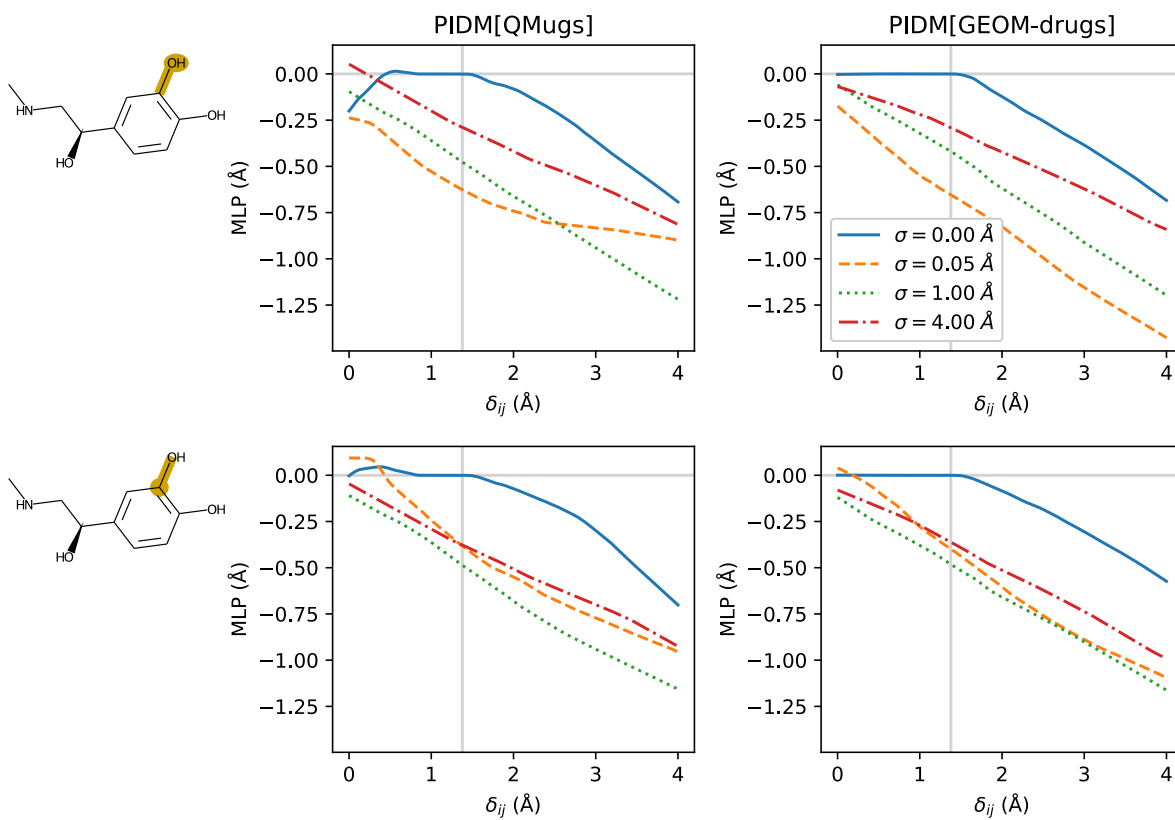


Figure 25: Example bond correction for the oxygen (top row) and carbon (bottom row) in a hydroxyl in adrenaline.

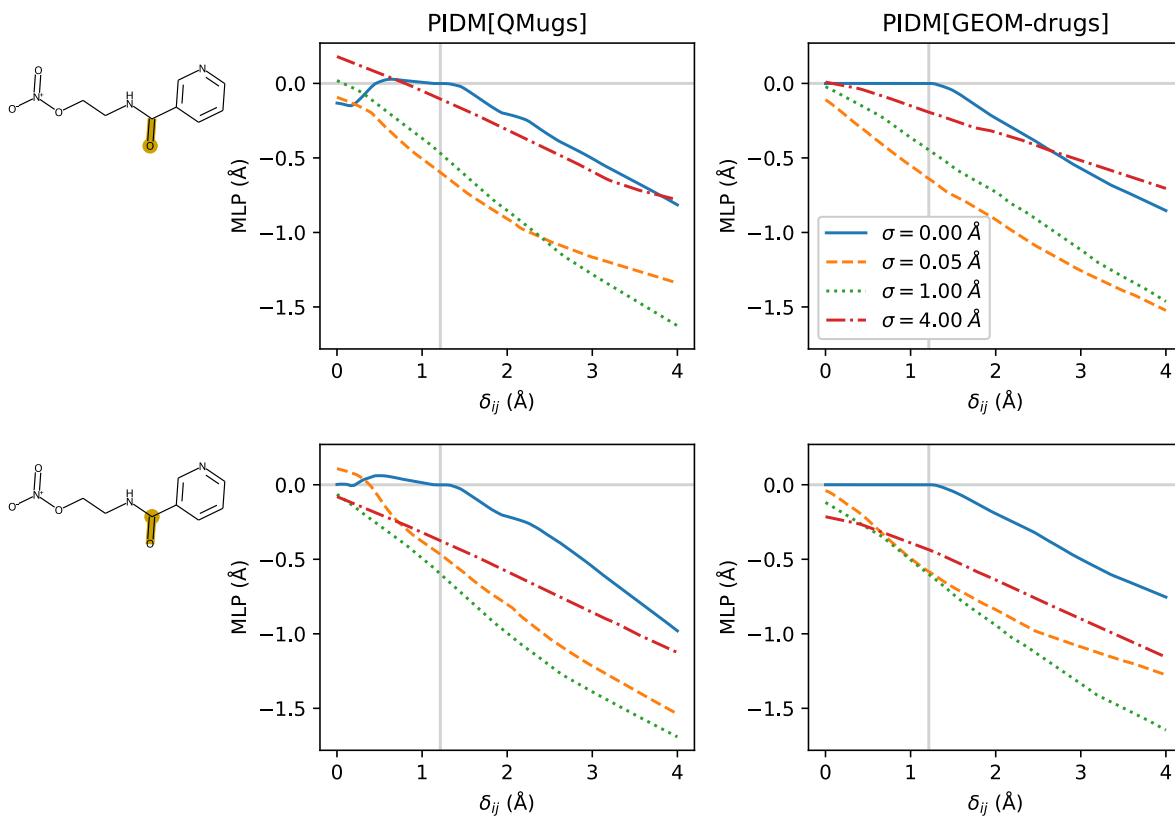


Figure 26: Example bond correction for the oxygen (top row) and carbon (bottom row) in an amide in nicorandil.

Bend component

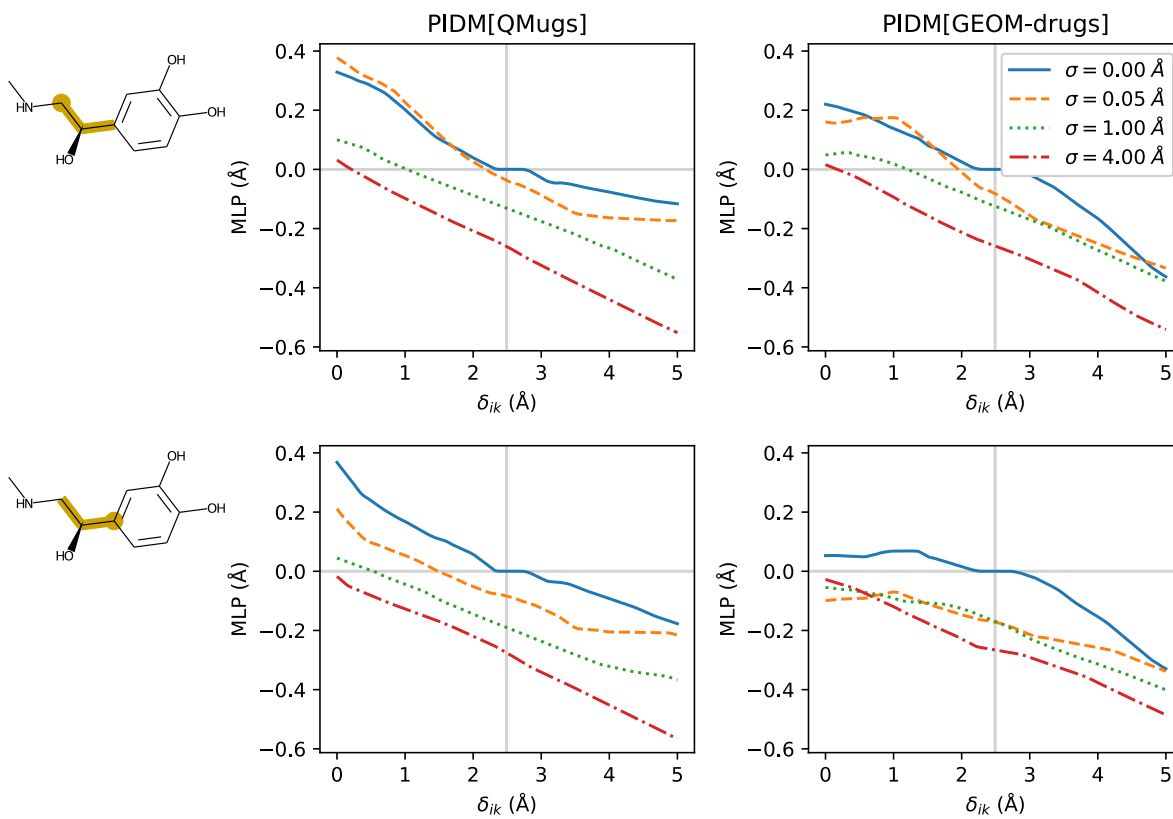


Figure 27: Example bend angle correction for an alkane in adrenaline.

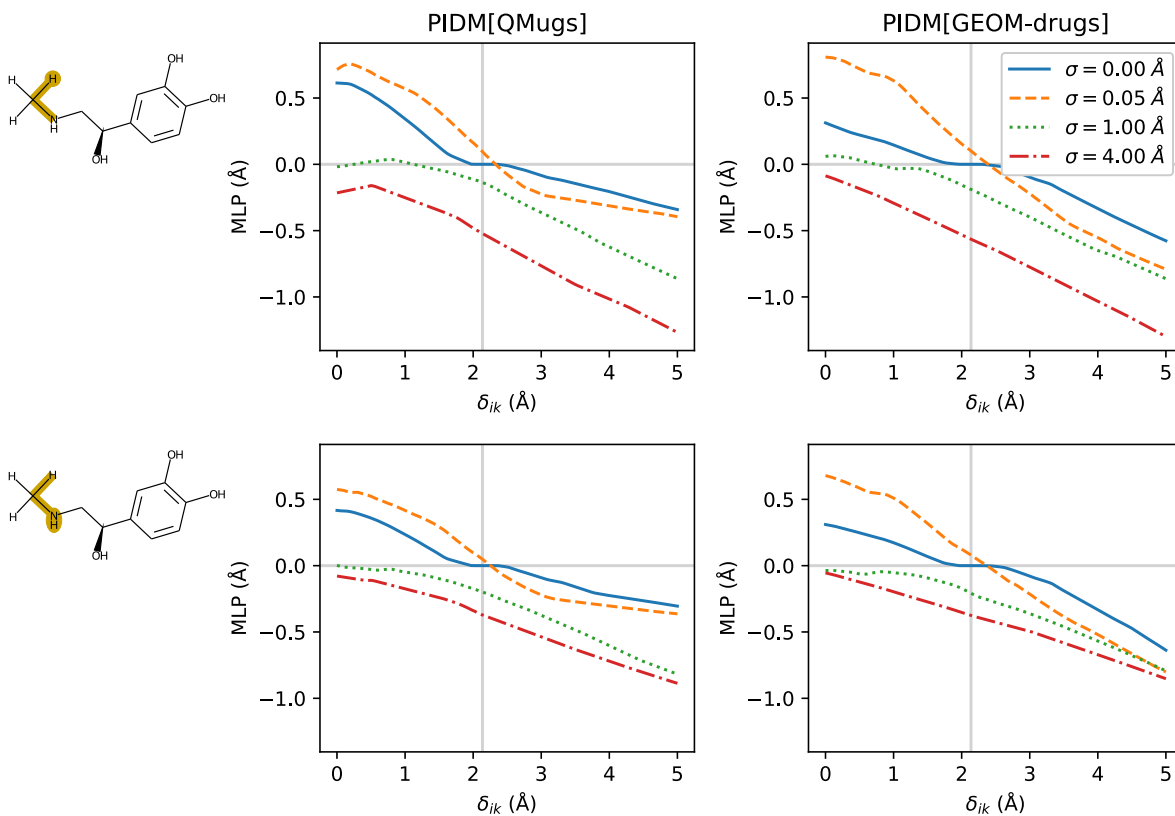


Figure 28: Example bend angle correction for hydrogen and nitrogen in the methylamine in adrenaline.

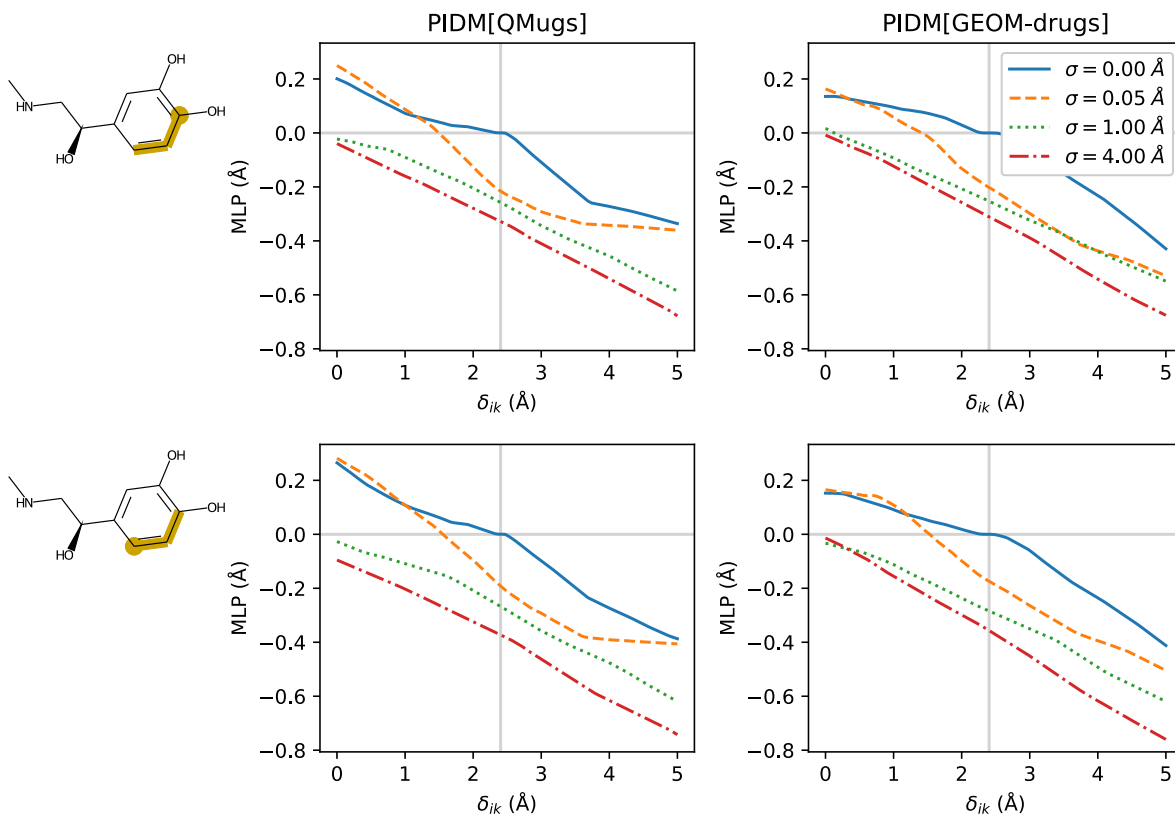


Figure 29: Example bend angle correction for carbons in the phenol ring in adrenaline.

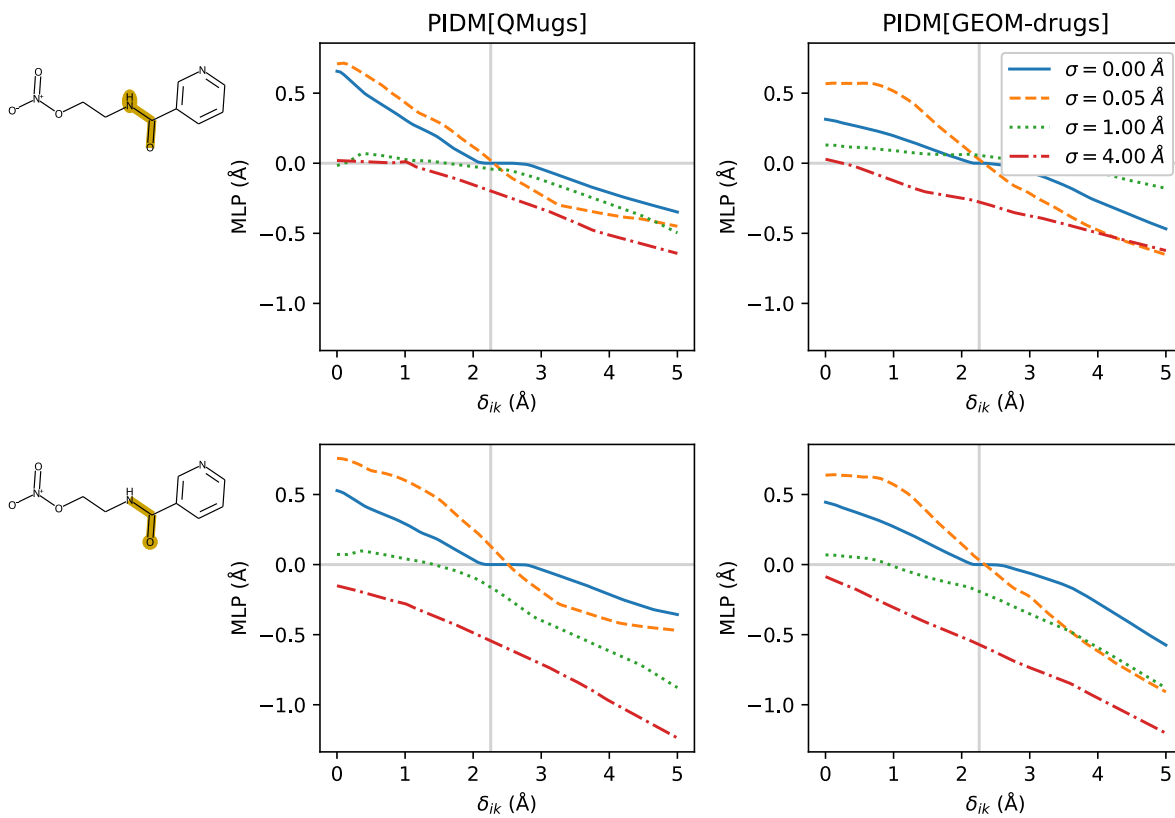


Figure 30: Example bend angle correction for the amide in nicorandil.

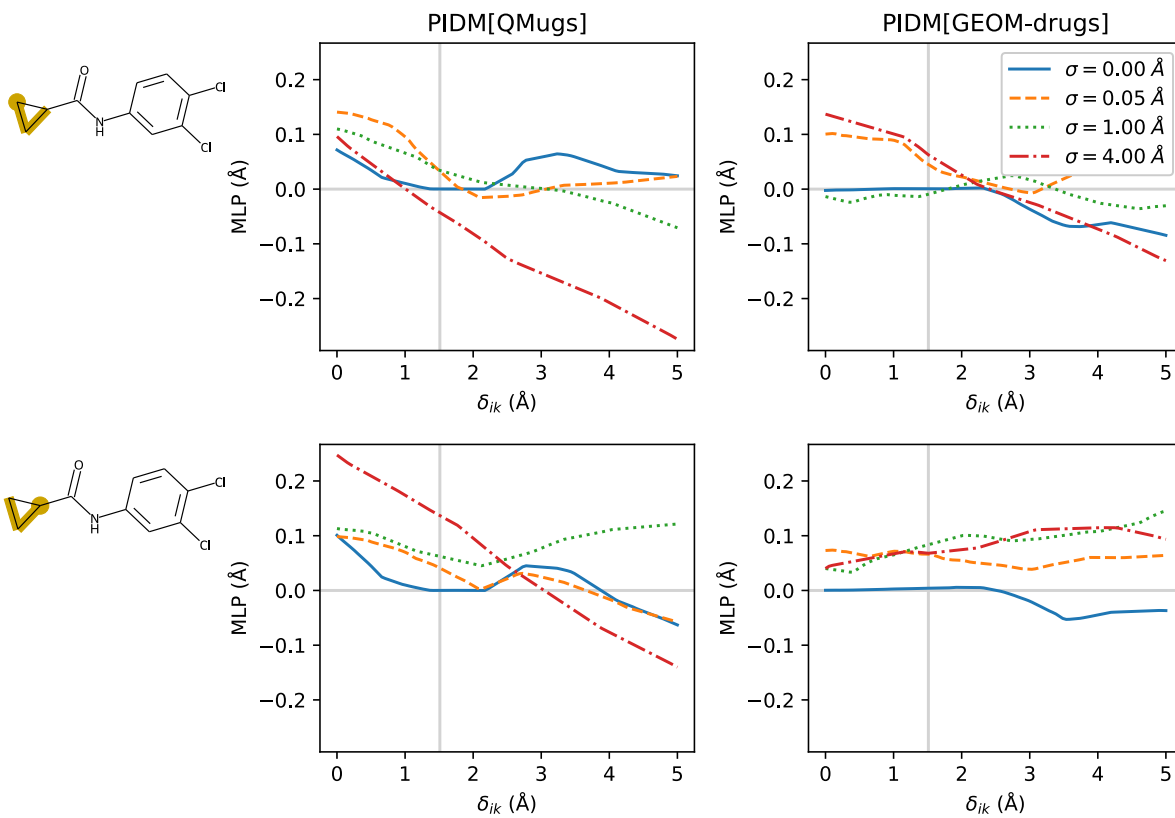


Figure 31: Example bend angle correction for carbons in the cyclopropyl of cypromid.

Proper torsion component

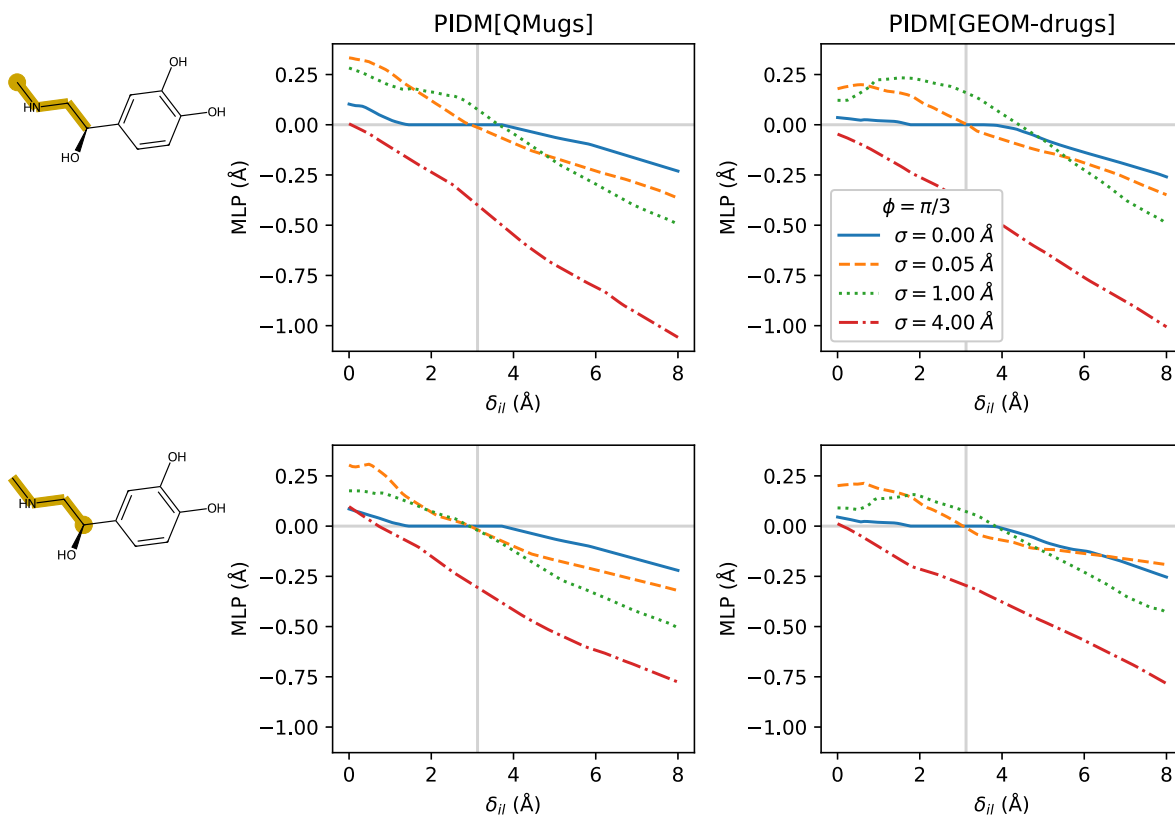


Figure 32: Example proper torsion angle correction for the methylethylamine in adrenaline.

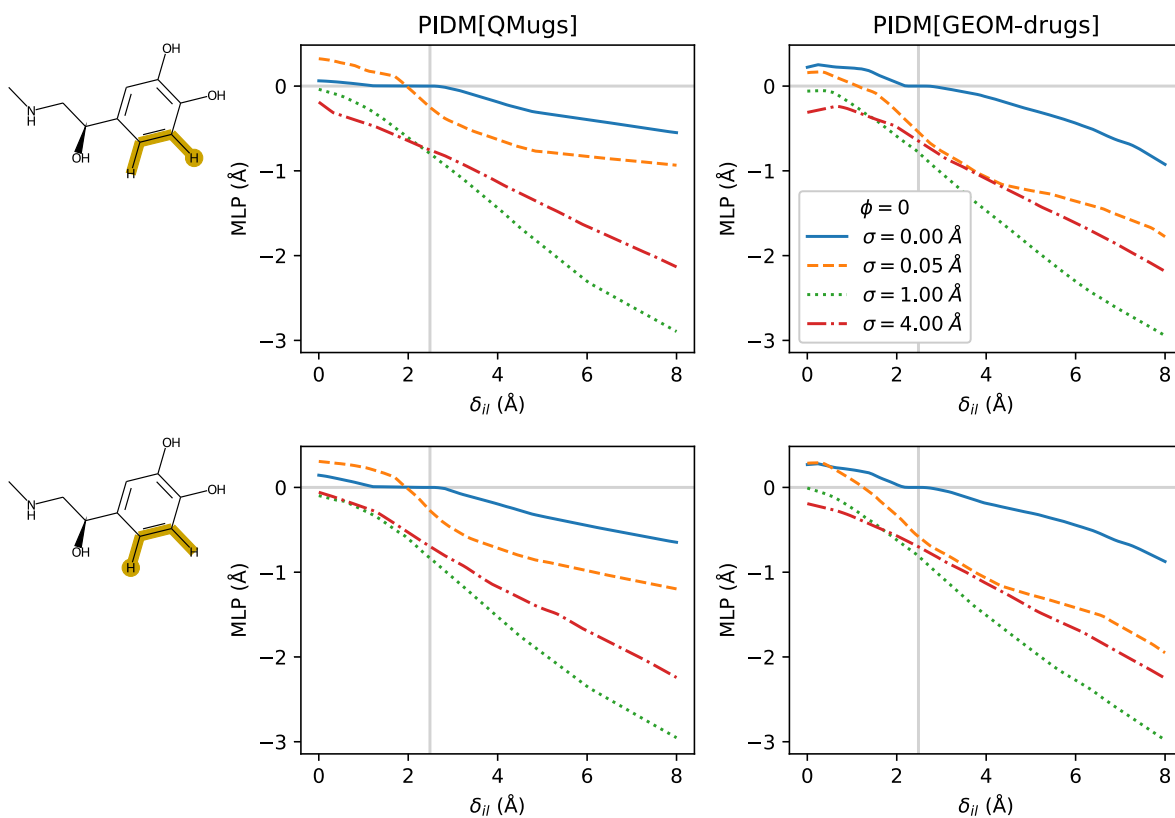


Figure 33: Example proper torsion angle correction for two hydrogens in the phenol ring in adrenaline.

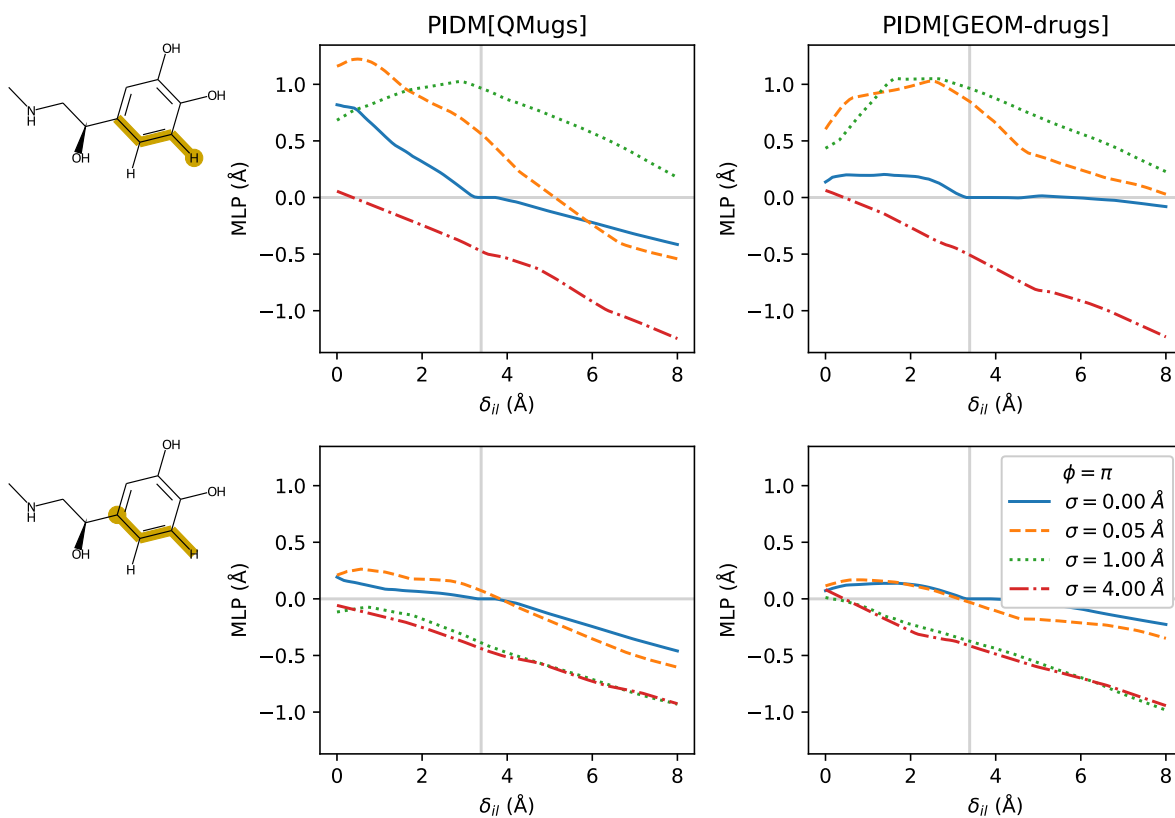


Figure 34: Example proper torsion angle correction for a hydrogen and a carbon in the phenol ring in adrenaline.

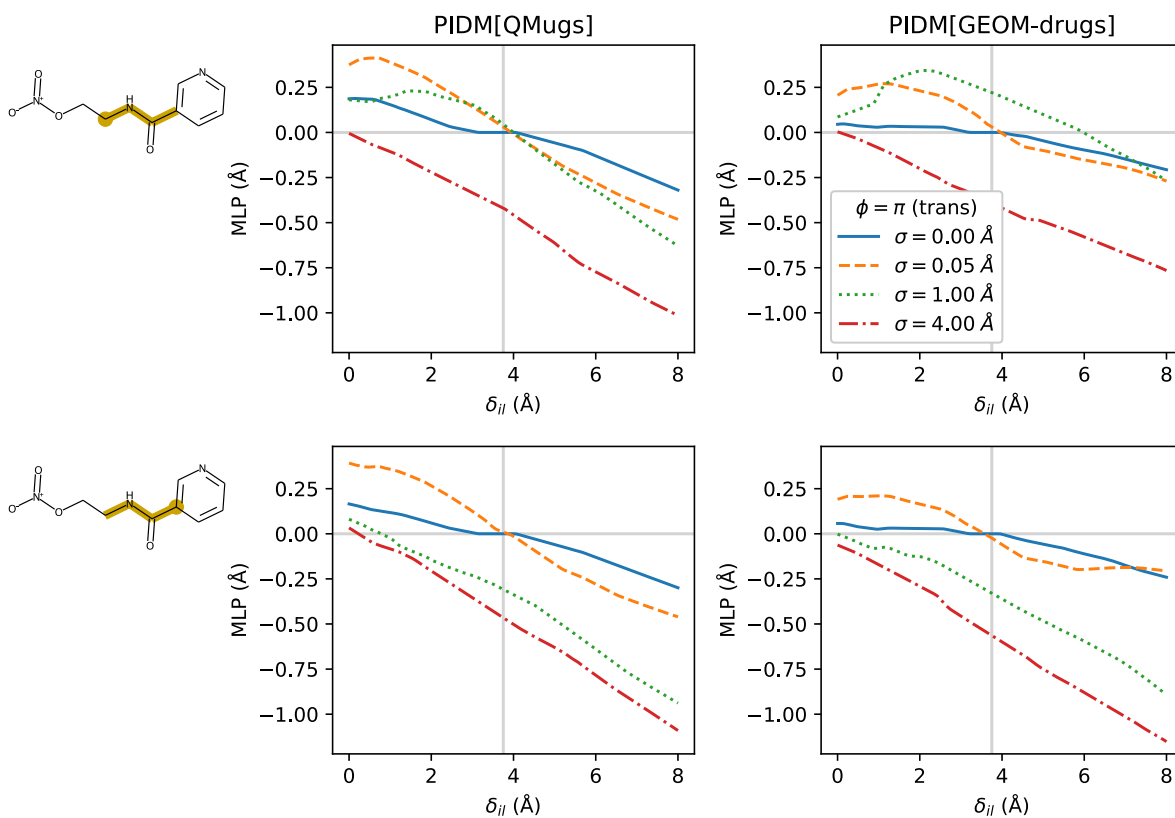


Figure 35: Example proper torsion angle correction for an amide in nicorandil in the trans configuration.

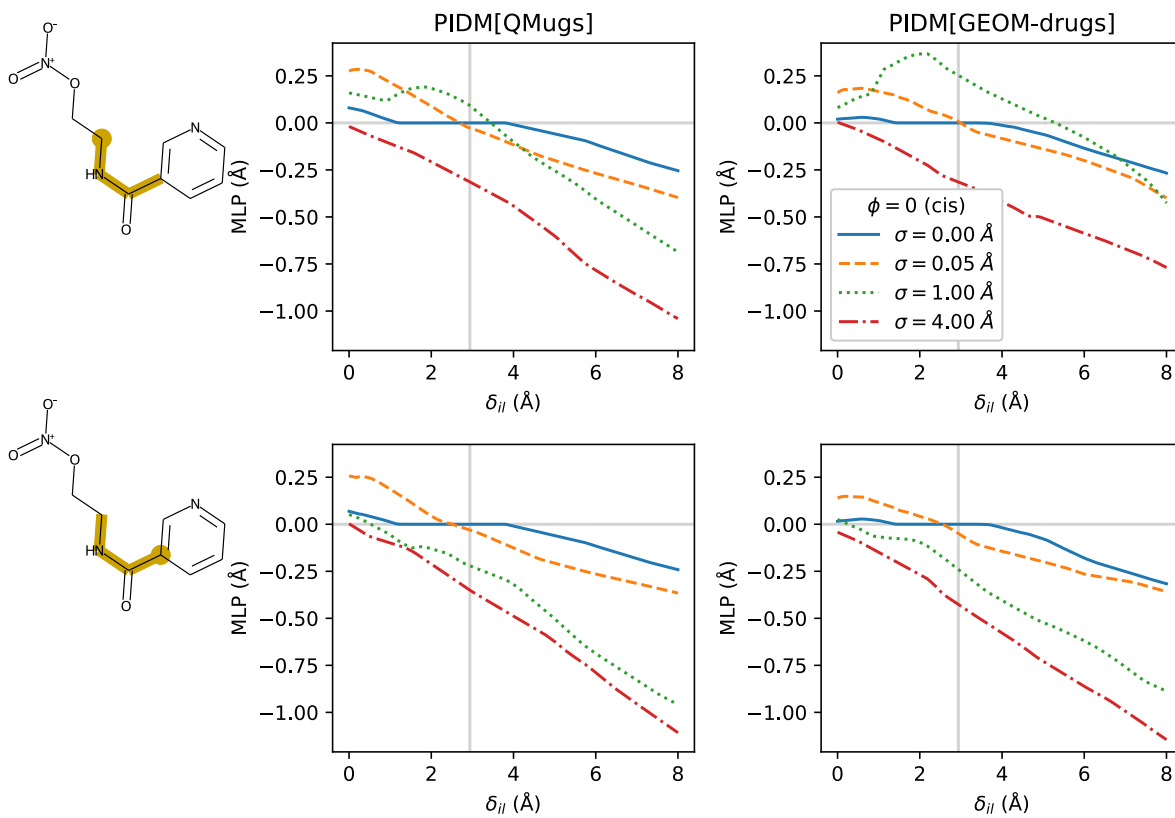


Figure 36: Example proper torsion angle correction for an amide in nicorandil in the cis configuration.

Chirality component

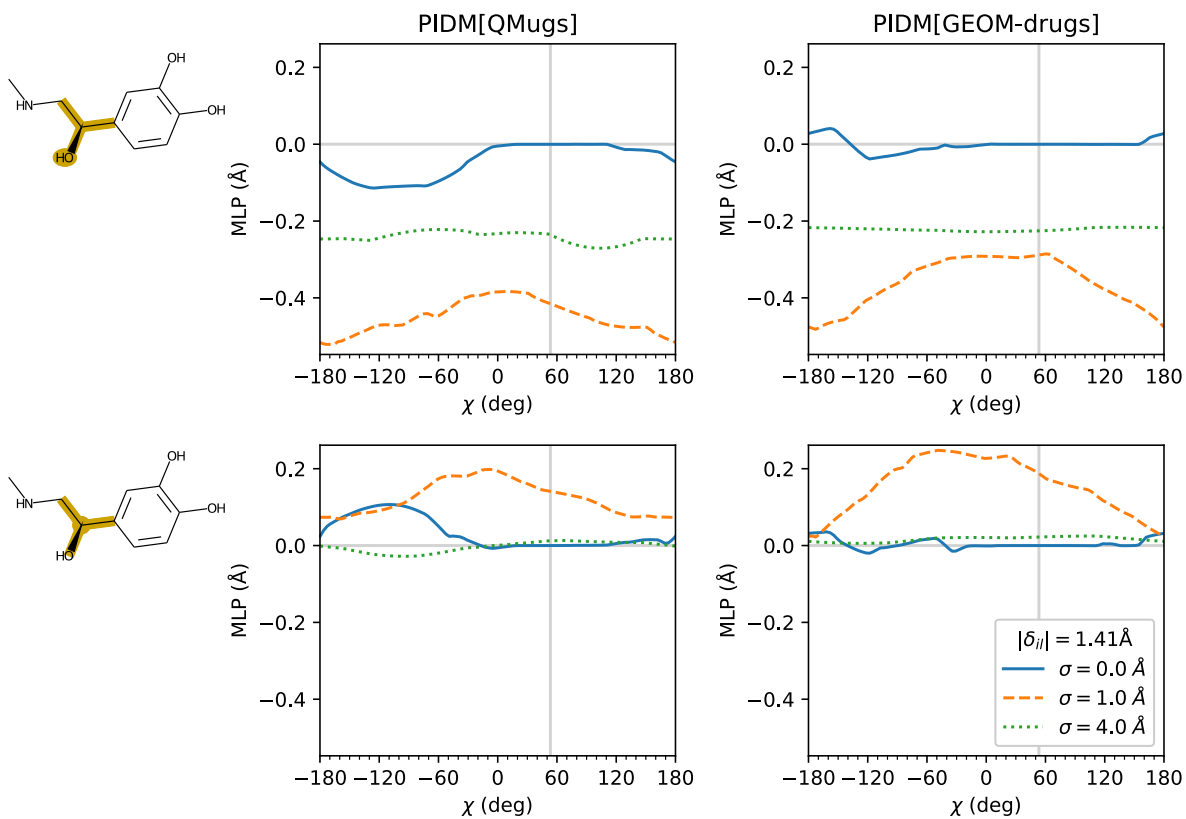


Figure 37: Example chirality correction for the hydroxyl on the chiral center of adrenaline. The chirality angle χ is sampled at a bond length of 1.41 \AA , corresponding to the GFN2-xTB prediction.

Cis-trans component

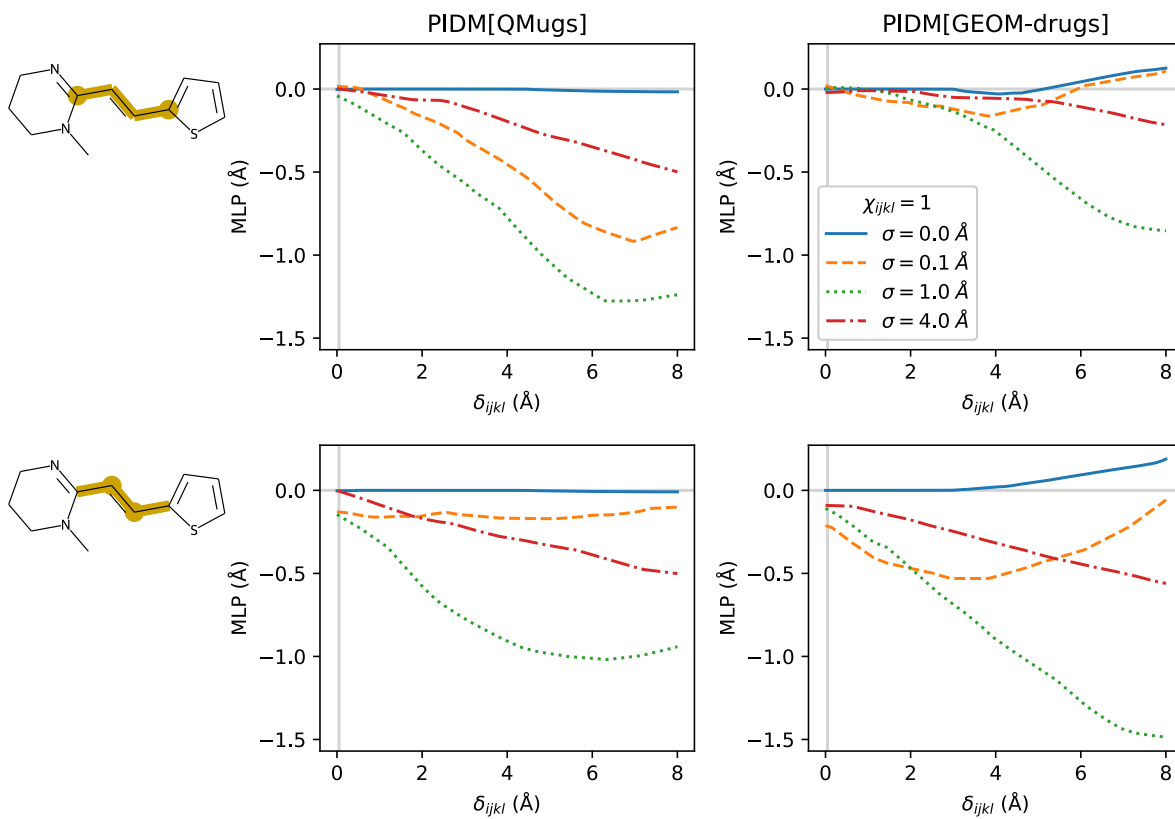


Figure 38: Example cis-trans correction for the carbons on the double bond of pyrantel.

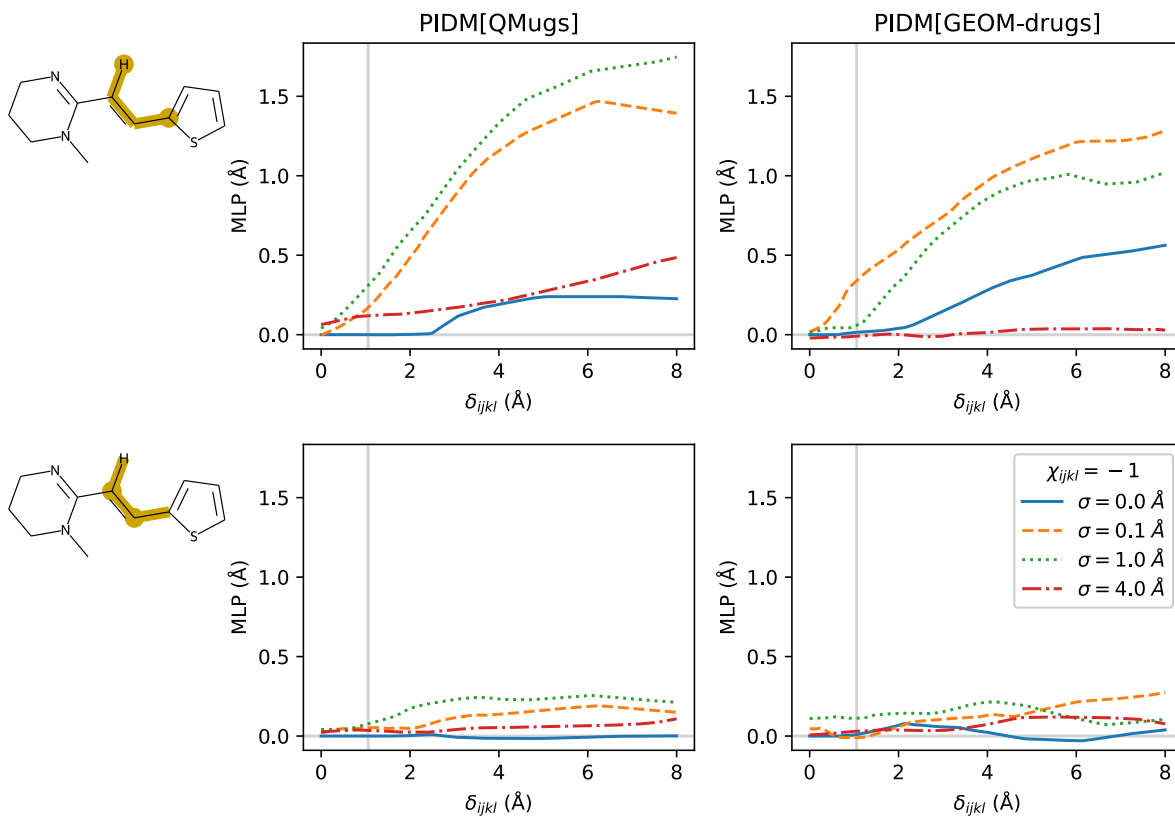


Figure 39: Example cis-trans correction for a hydrogen on the double bond of pyrantel.

Additional example output

The following are conformers generated from molecules selected randomly from the benchmark dataset. No filtering has been applied. In all of these figures, the second column from left (grey background) is the first conformer from QMugs. Shown on the right are the first four conformers generated by PIDM. All molecule renderings are oriented by principal component.

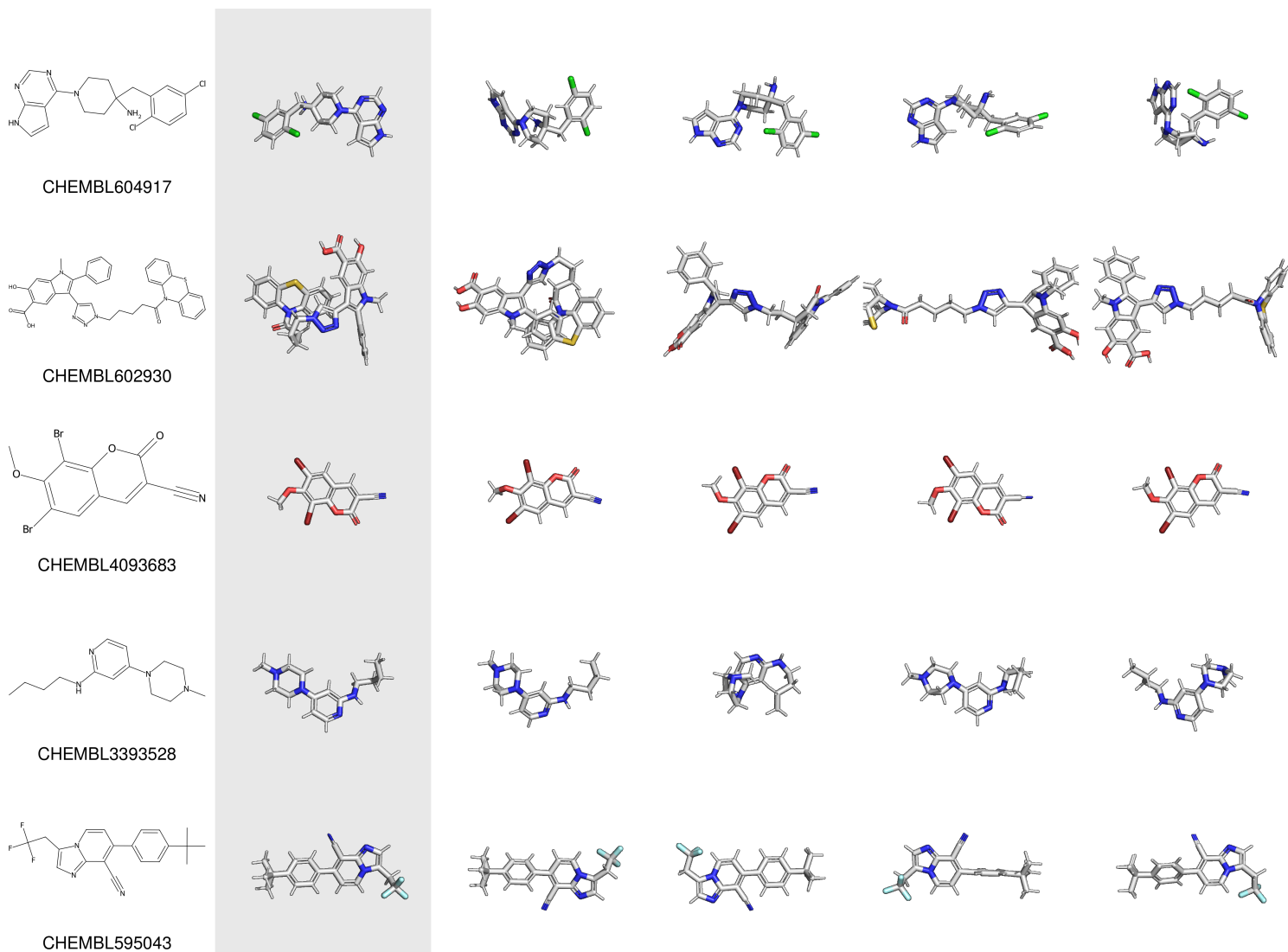


Figure 40: Example conformer output, randomly selected, for PIDM[QMugs], using stochastic generation and 500 steps.

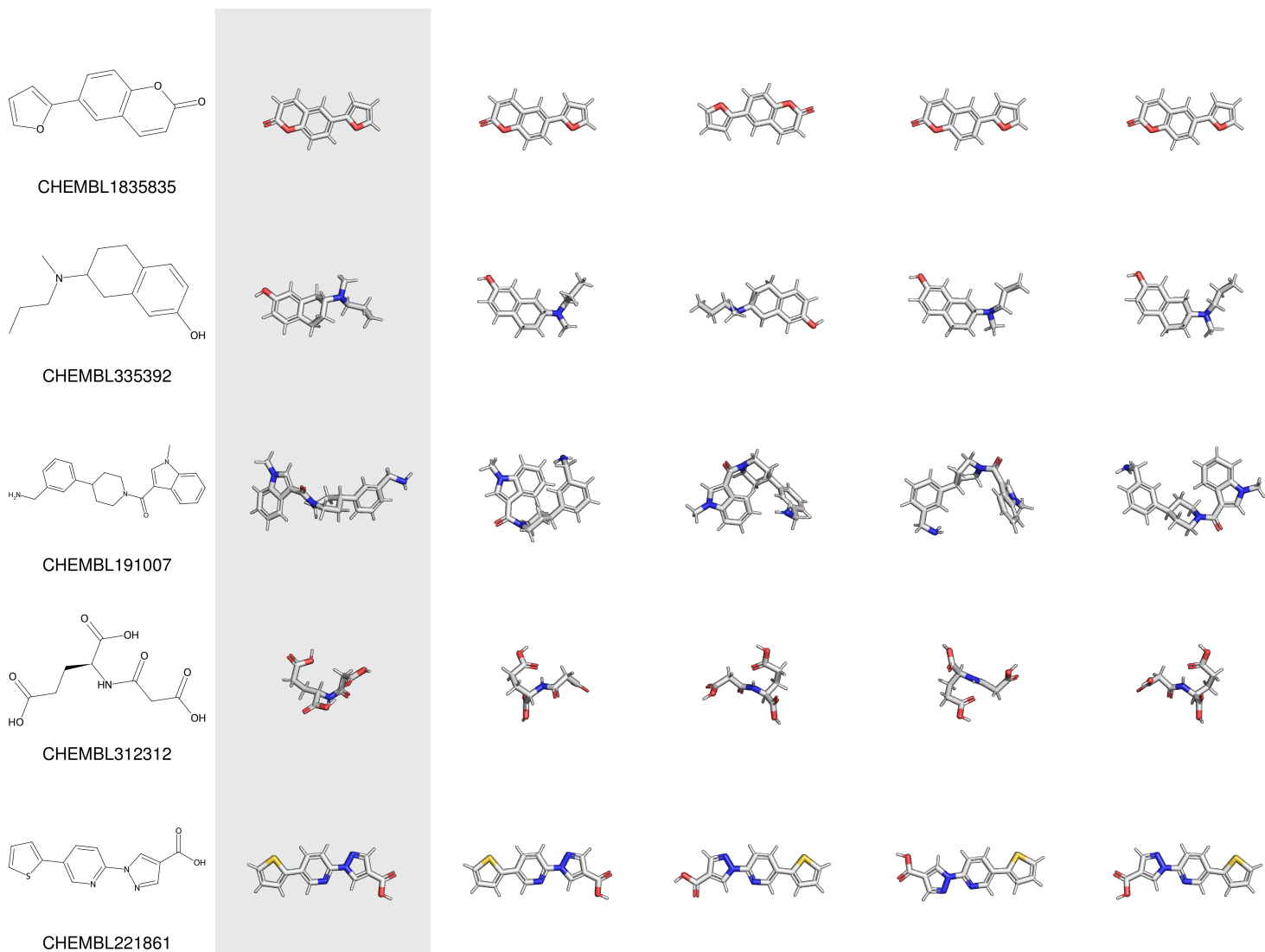


Figure 41: Example conformer output, randomly selected, for PIDM[GEOM-drugs], using deterministic generation and 500 steps.

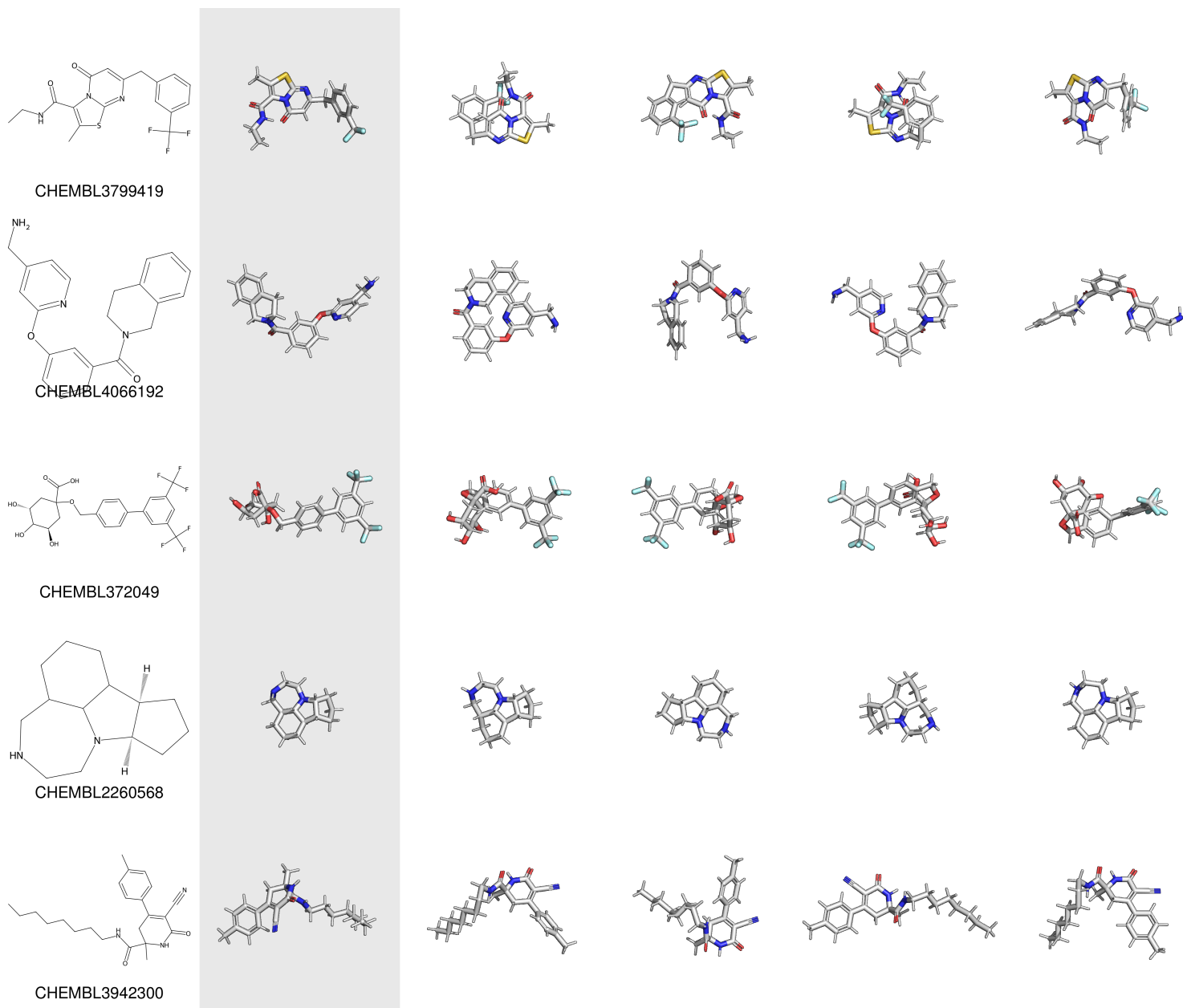


Figure 42: Further example of conformer output, randomly selected, for PIDM[QMugs], using deterministic generation and 500 steps.

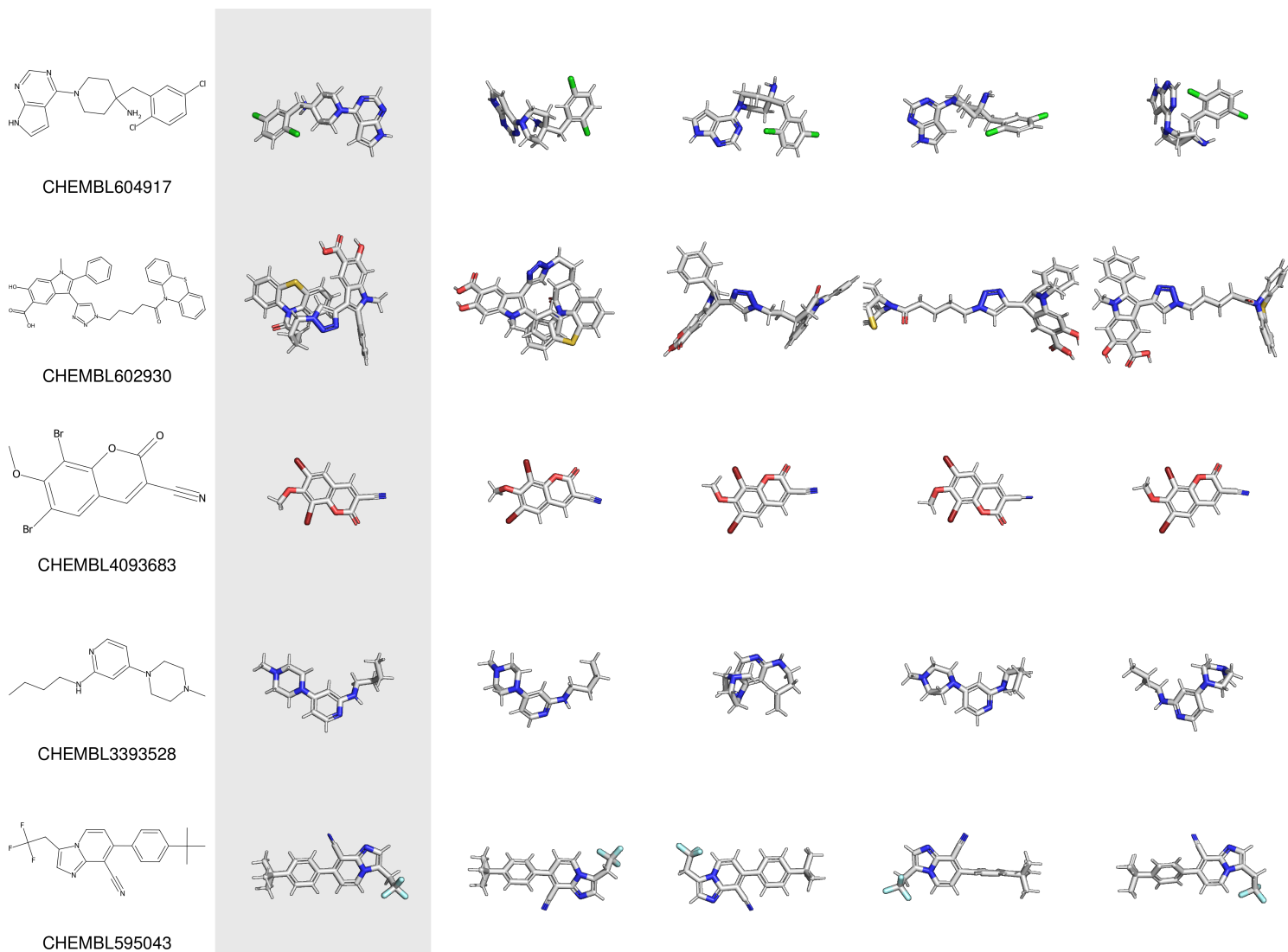


Figure 43: Further example conformer output, randomly selected, for PIDM[QMugs], using deterministic generation and 500 steps.

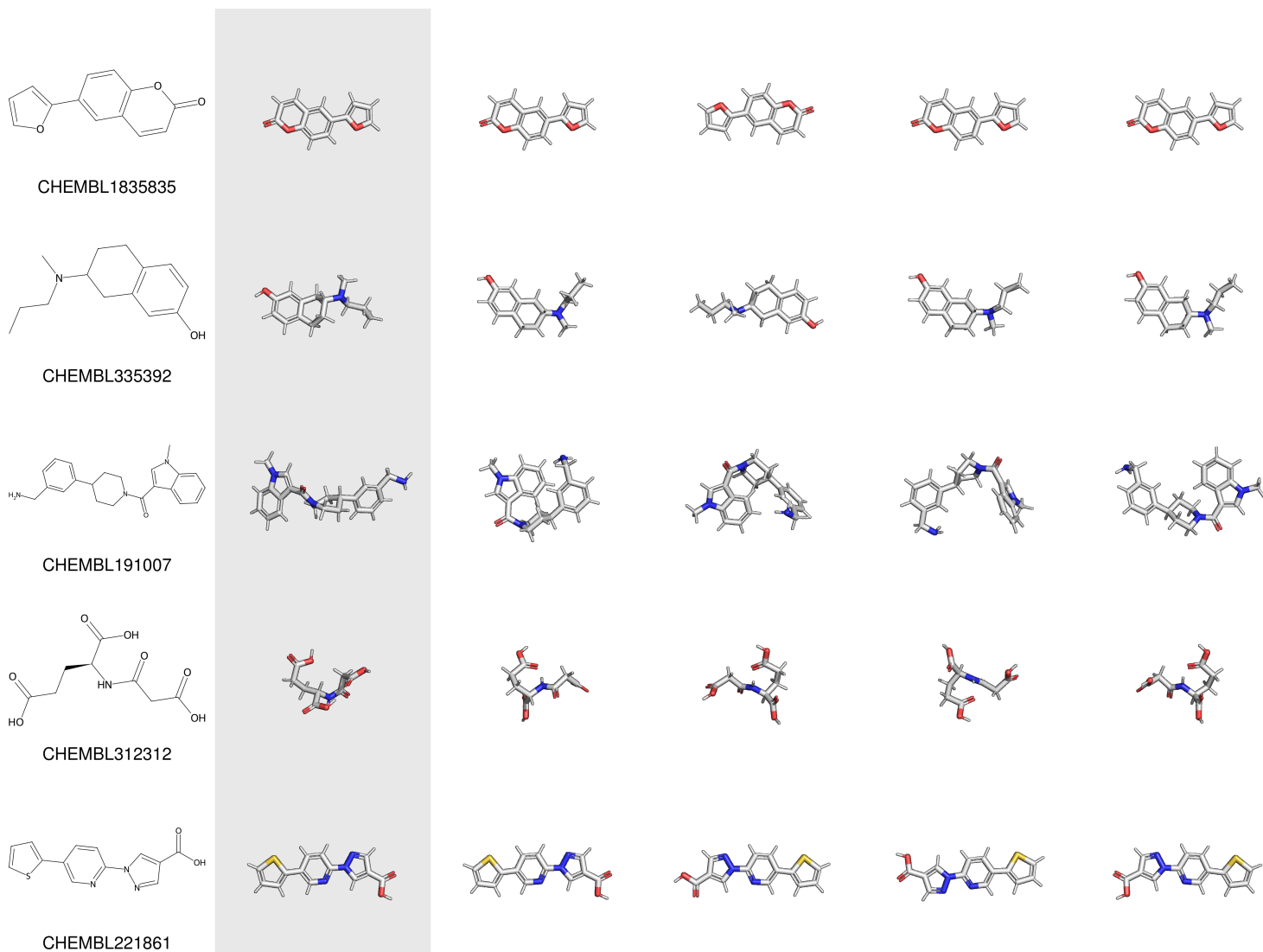


Figure 44: Further example conformer output, randomly selected, for PIDM[QMugs], using deterministic generation, 500 steps, and repulsion of $\eta = 1$.

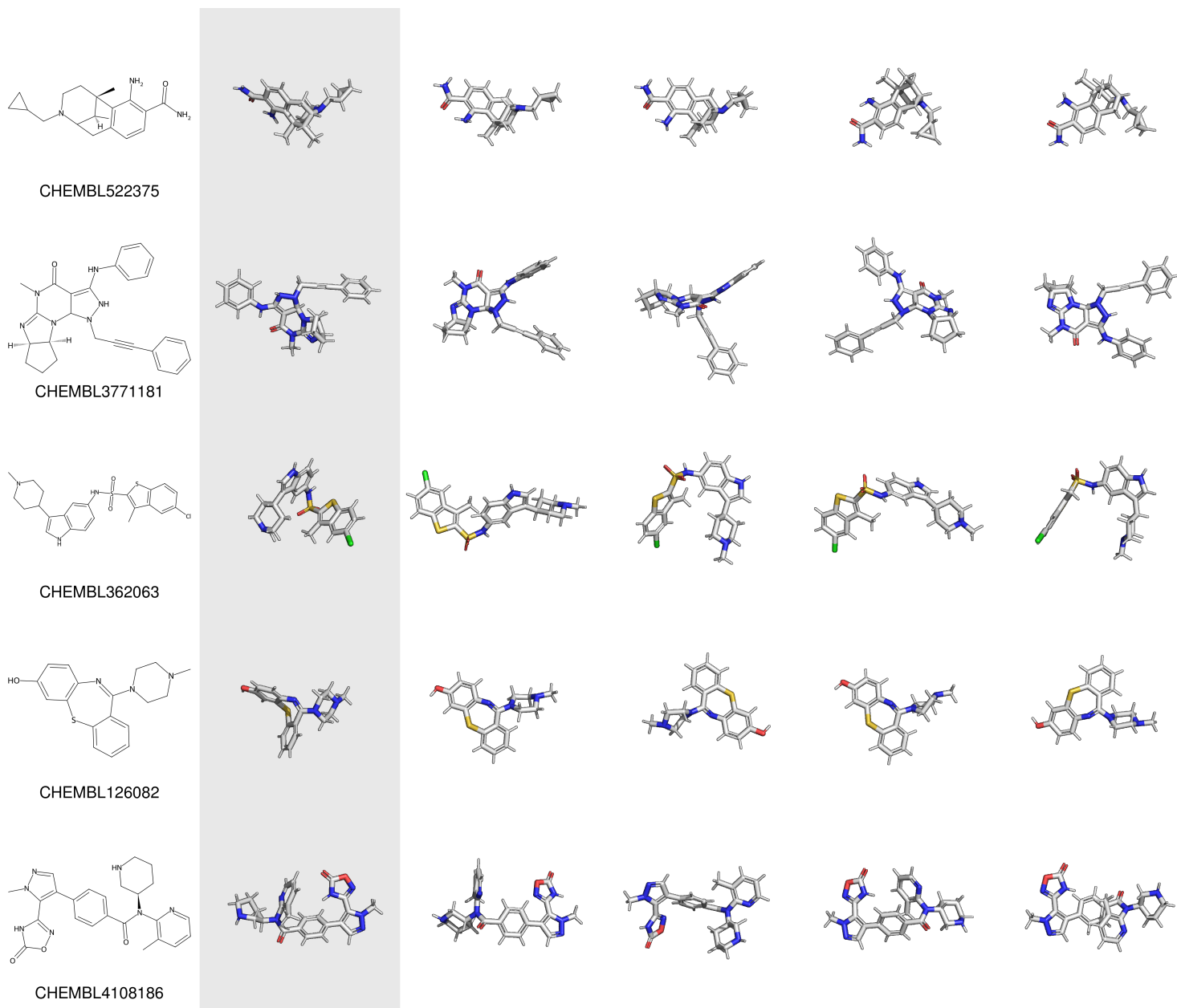


Figure 45: Further example conformer output, randomly selected, for PIDM[QMugs], using deterministic generation, 500 steps, and repulsion of $\eta = 1$.